



NAVAL
POSTGRADUATE
SCHOOL

Spacecraft Robotics
LABORATORY

Spacecraft Dynamics, Guidance & Control: Analysis, Simulations, Experimentation

“An overview of research at the NPS-SRL
+
refresher (intro) to RB rotational mechanics”

Dr. Marcello Romano, mromano@nps.edu, mmromano@stanford.edu

Professor, Mechanical and Aerospace Engineering Department & SSAG
Founder/Director, Spacecraft Robotics Laboratory
Naval Postgraduate School, Monterey, California

Currently on Sabbatical at Stanford Aero/Astro until Dec 2018

Prof. D'Amico's Class
@ Stanford
6 June 2018

Romano's Lab & Group Main Facts

SRL Founder (2004), Director & PI/PM: Prof. Marcello Romano,

Research Team members:

Dr. Josep Virgili, NRC Postdoctoral Research Associate

Dr. Ayansola Ogundele, NRC Postdoctoral Research Associate

PhD Candidates: Capt Costantinos Zagaris, Ms Alanna Sharp

MS Students: LT Katrina Alsup, LT Justin Komma, LT Jessica Shapiro, LT Tristan Struckmeier, LT Fabian Stracker

Selected Alumni

Postdocs: Dr. Bevilacqua (UF); Dr. Wilde (FIT); Dr. Ciarcia' (USD), Dr. Park (UNM)

Ph.D.: Drs. Bevilacqua, Hall, McCamish, Boyarko, Chesi (Planetlab), Zappulla (AFRL), Tavora

MS: >30 DoD Officers.

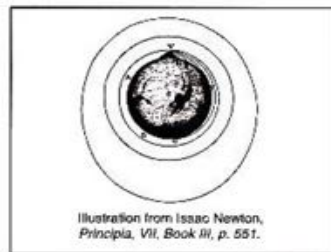
Sponsors:



Research Foci

Autonomous Spacecraft DGN&C

ASTRODYNAMICS	ORBITAL ROBOTICS	S/C ENGINEERING
Attitude Maneuver Proximity Maneuver	Multi-body S/C Physically interacting S/C	Dynamic Lab Test-beds Prototype GN&C RT-SW Prototype HW
<i>Optimal / Agile maneuver Proximity maneuver Propellantless maneuver</i>	<i>Docking/grasping, Assembly Servicing, Debris removal Resilient systems</i>	<i>DGN&C testing Small satellites technology New systems/subsystems</i>



Priority: education at university postgraduate level, archival/quality publications, patents

Philosophy: problem oriented, theory to applications, analysis/ simulations/ lab & flight experiments.

Overview of selected research topics

- 1) Spacecraft Engineering & Technology
-Development of HIL Test-beds for Spacecraft Proximity and Attitude Maneuvering (GN&C)
- 2) Orbital Robotics
-Design/test G&C Algorithms for S/C Proximity & Attitude Maneuvering
- 3) Space Flight Mechanics
-Using Residual Aero-Drag for Attitude Maneuvers
-Seeking & Using Exact Solutions of Rigid Body Motion

HIL Lab Testing of S/C Maneuvering

Rationale:

Critical tool for performing research and supporting university education.
Relative low-cost/low-risk bridge between Numerical Simulation and Flight

Three types of HIL Lab Testing:

1. HIL Dynamic Lab Testing:

- Linear and/or angular accelerations are generated by actuators—e.g. jet thrusters or RWs—on-board the test vehicle (*self-motion*)
- spurious forces (not representative of actions on orbit) are minimized

2. HIL Kinematic Lab Testing:

- Linear and/or angular accelerations are generated by actuators external to the on-board test vehicle (*imposed motion*)

3. HIL Static Lab Testing:

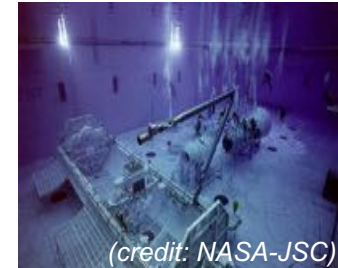
- a.k.a. flat-sat or breadboard components testing.
- the test-vehicle or components are tested statically

HIL Dynamic Lab Testing of S/C Maneuvering

Roto-translational (proximity) maneuvering

1) *Floating in neutral buoyancy pools (JSC, UM, EAC)*

per vehicle: {dof: 6, config. space: SE(3), residual dist.: $\sim 10^{-1}$ g}



2) *Floating over horizontal surfaces via flat air-bearing*

(e.g. NPS, Ames, MIT, NRL, Stan.U, UF, Technion, Thales)

per vehicle: {typical: 3dof, $R^2 \times R, \sim 10^{-4}$ g}, {also possible: 5dof, $R^2 \times SO(3)$ }



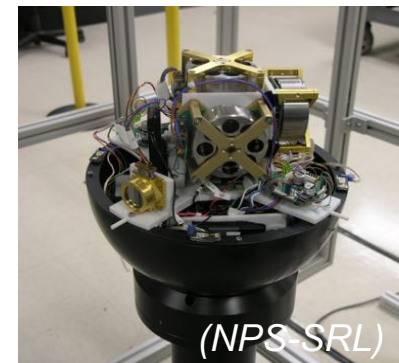
(NPS-SRL)

Rotational (attitude) maneuvering

Floating spherical air-bearing,

a.k.a. *dynamic three axis simulator* (e.g: AFRL, NPS)

{3dof, SO(3), $\sim 10^{-3}$ Nm}



(NPS-SRL)

Application: experimental testing of:

RT GN&C algorithms, MB & contact dynamic models,
actuators/sensors H/W and S/W

HIL Kinematic Lab Testing of S/C Maneuvering

Roto-translational (proximity) maneuvering

1) *Cartesian Robotic Crane System*
(e.g.: *NRL, TUM*)

per vehicle: {dof: 6, motion type: SE(3)}



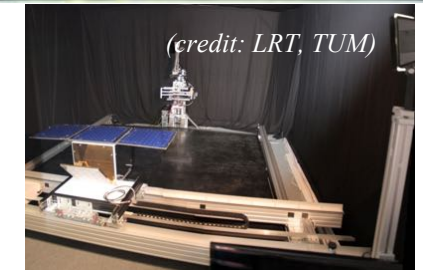
2) *Rail system* (e.g.: *EPOS, ESA, Stanford*)
per vehicle: {typical: 6dof, motion type: SE(3)}



(credit: EPOS)



(credit: ESA)



(credit: LRT, TUM)

Rotational (attitude) maneuvering

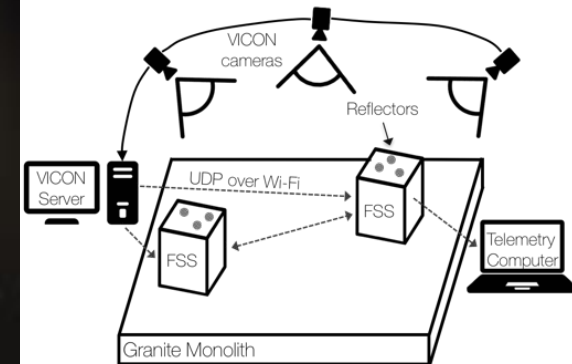
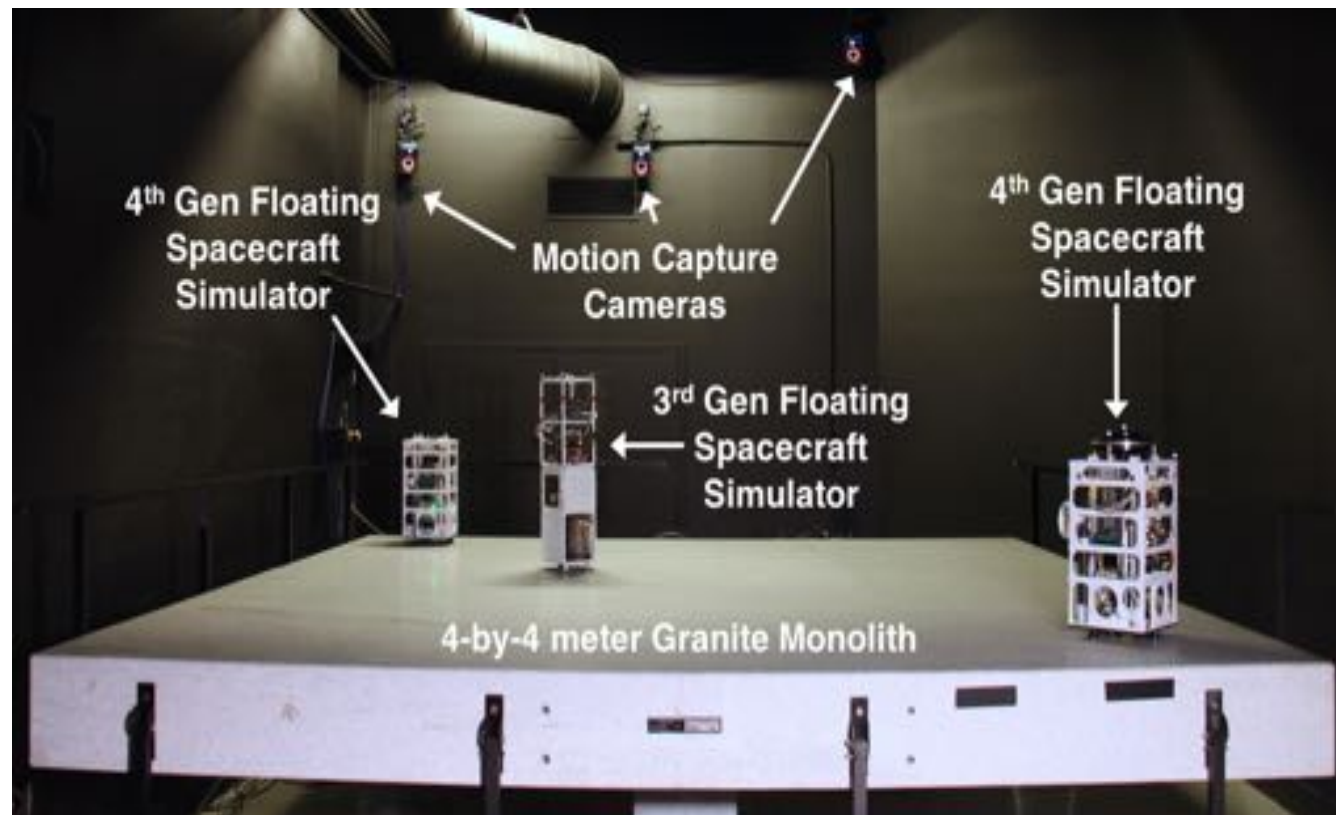
Rotational stage (a.k.a. kinematic three-axes simulator) {3dof, SO(3)}

Application: experimental V&V of:
Navigation algorithms, Sensor H/W and S/W

The NPS POSEIDYN Test Bed (2004-2018)

POSEIDYN: Proximity Operation of Spacecraft: Experimental hardware-In-the-loop DYNAMIC simulator

Elements: 1) granite table, 2) autonomous floating S/C simulators, 3) metrology system.



Goals: testing of dynamic models / GN&C algorithms, graduate students education

[Ref: Zappulla, Virgili-Llop, Zagaris, Park, Romano, *POSEIDYN Air-Bearing Test Bed for Experimental Evaluation of Autonomous Spacecraft Proximity Maneuvers*. *Journal of Spacecraft and Rockets*, 2017]

The NPS POSEIDYN Test Bed: Hardware

Five generations of Spacecraft Simulators have been developed:

- ◆ 1st Gen: Uses DARPA Orbital Express Docking Interface
- ◆ 2nd Gen: Vectorable thrusters and a miniature CMG
- ◆ 3rd Gen: Polycarbonate structure, Lavalle nozzles
- ◆ 4th Gen (2016-2017): Increased modularity and standardized docking interface
- ◆ NEW ! 5th Gen (2018): *under development, 5 U and 6 U size simulators, heterogeneous computer, open hardware distribution*

2004-2006



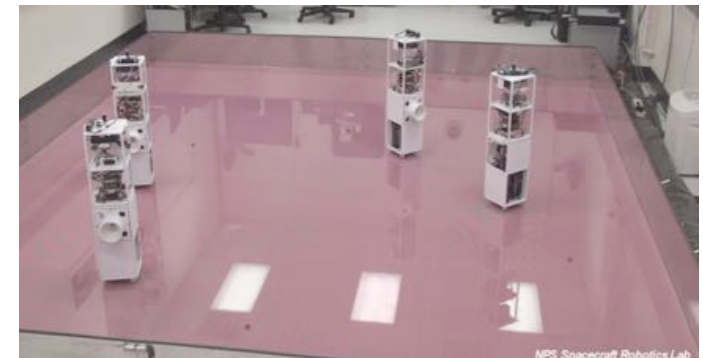
1st Generation S/C Simulators
65 Kg, 0.45 X 0.45 X 1 m
(2 units built)

2006-2009



2nd Gen. simulator
37 Kg, 0.3 X 0.3 X 0.7 m
(1 unit built)

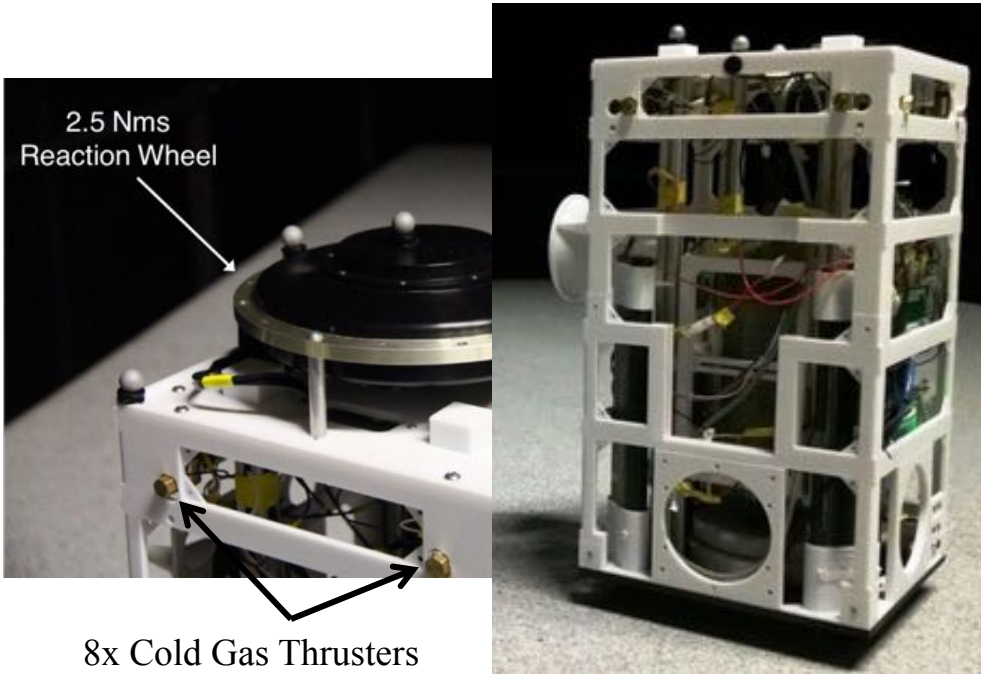
2008-2016



3rd Gen. Simulator
9.5 Kg, 0.2X0.2X0.8 m
(4 units built)

4th Gen Floating Spacecraft Simulator (FSS)

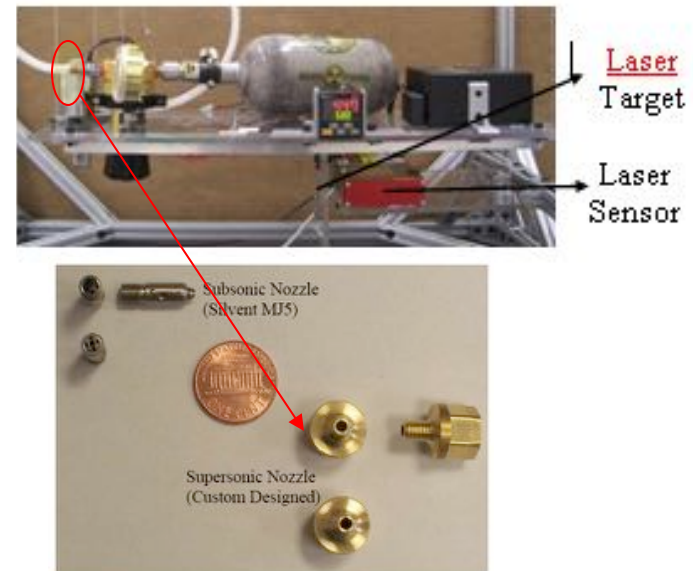
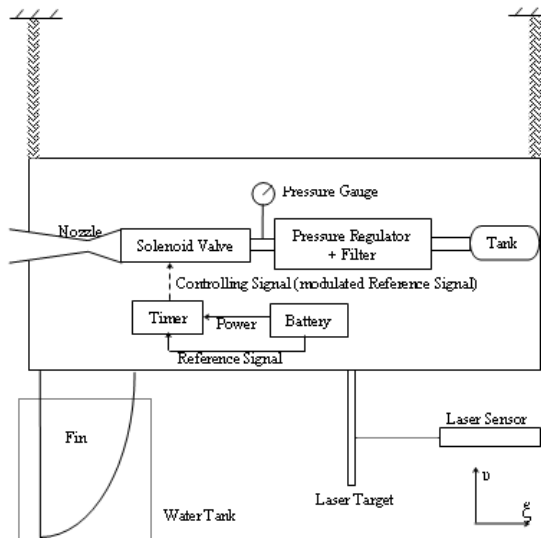
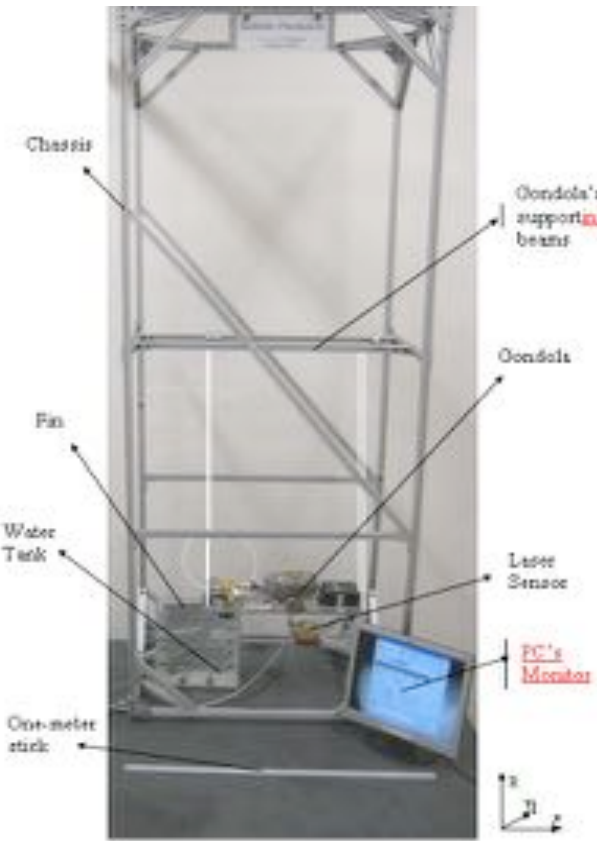
- ▶ Each self-contained FSS is designed to simulate the GN&C capabilities of a typical spacecraft
- ▶ 3 air pads are used to lift the FSS approximately $5\mu\text{m}$ (air supplied via on-board compressed air tank)
- ▶ 32-bit 1.6 GHz Intel Atom PC-104
- ▶ 8 cold gas 0.1 N thrusters, 0.1 Nm, 2.5 Nms RW



Parameter	Value
Mass, wet	$9.882 \text{ kg} \pm 0.001 \text{ kg}$
Mass, dry	$9.465 \text{ kg} \pm 0.001 \text{ kg}$
Dimensions	$0.27 \times 0.27 \times 0.52 \text{ m}$
Estimated MOI	0.2527 kg m^2
MOI StDev	0.0115 kg m^2

Autonomy (air, max firing): ~20 min
Mean Linear Residual Acceleration: $3.81 \times 10^{-4} \text{ m/s}^2$ (0.039 mG)
Mean Rotational Residual Acceleration: $7.25 \times 10^{-3} \text{ °/s}^2$

Supersonic nozzle development/characterization



Experimental results: characterization of the subsonic nozzle with $\Delta T_1=0.1$ s (15 repetitions).

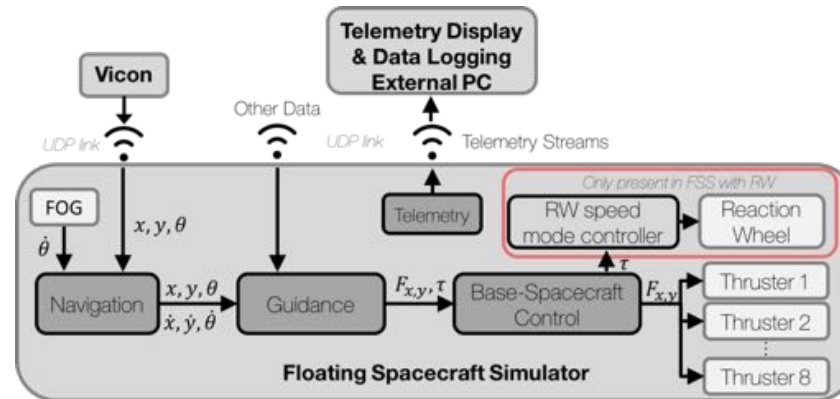
Pressure, MPa (psi)	Thrust, N	Mass Flow Rate, 10^{-4} kg/s	Specific Impulse, s
0,345 (50)	$0,118 \pm 0,003$	$6,2 \pm 0,2$	$19,4 \pm 0,5$

Experimental results: characterization of the supersonic nozzle with $\Delta T_1=0.1$ s (15 repetitions).

Pressure, MPa (psi)	Thrust, N	Mass Flow Rate, 10^{-4} kg/s	Specific Impulse, s
0,138 (20)	$0,062 \pm 0,002$	$1,802 \pm 0,200$	$35,1 \pm 1,2$
0,207 (30)	$0,089 \pm 0,002$	$2,603 \pm 0,200$	$34,9 \pm 0,8$
0,276 (40)	$0,112 \pm 0,002$	$3,203 \pm 0,200$	$35,7 \pm 0,7$
0,345 (50)	$0,136 \pm 0,004$	$4,004 \pm 0,200$	$34,6 \pm 1,0$
0,414 (60)	$0,159 \pm 0,004$	$4,605 \pm 0,200$	$35,2 \pm 0,9$

[REF: Lugini, Romano, A Ballistic-Pendulum Test Stand to Characterize Small Cold-gas Nozzles, Acta Astronautica. 2009.]

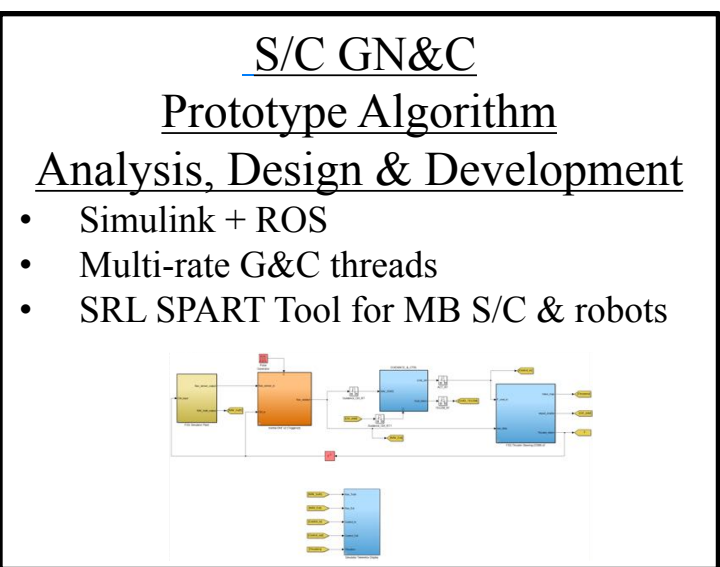
The NPS POSEIDYN Test Bed: Software



- ▶ Multi-rate GNC software (compiled modular Simulink code) runs atop a Real-time Linux OS (currently: 10.04 Ubuntu with PREEMPT-RT patched kernel v2.6.33. Benchmarked patched kernel max OS latency: **100µs** vs max normal kernel latency > **13 ms**)
- ▶ On-board GNC software broken up into 4 main sections:
 - ◆ Navigation, Guidance, Control, Telemetry
- ▶ Navigation block utilizes a discrete Kalman Filter (DKF) to fuse the Vicon and Fiber Optic-Gyro (FOG) data
- ▶ Control block maps the requested control input to the appropriate thrusters and modulates them to create the desired effect
- ▶ TCP/UDP Link allows for Vicon Measurements sharing, Intra-FSS communication/data sharing, telemetry for collection and presentation

Ref: http://pengutronix.de/software/linux-rt/debian_en.html

GN&C Prototype Software development / testing



GN&C Executable Modules

Off-line execution on PCs
(e.g. for V&V and/or Mission Analysis)

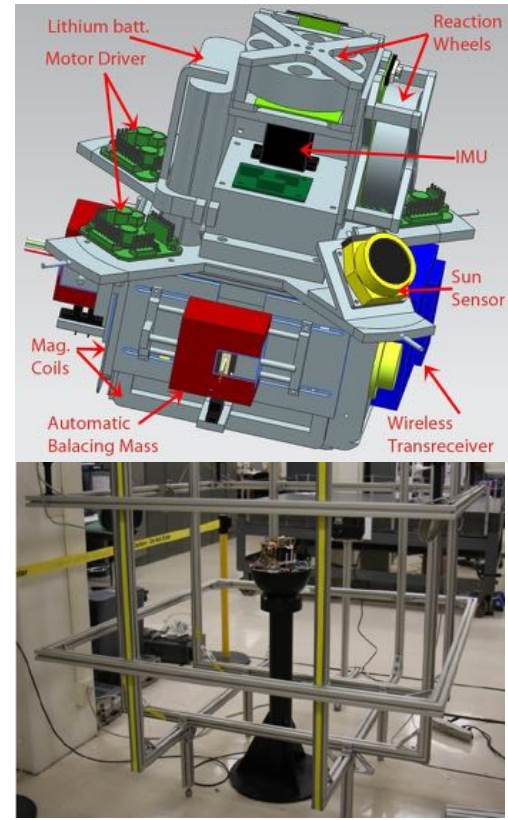
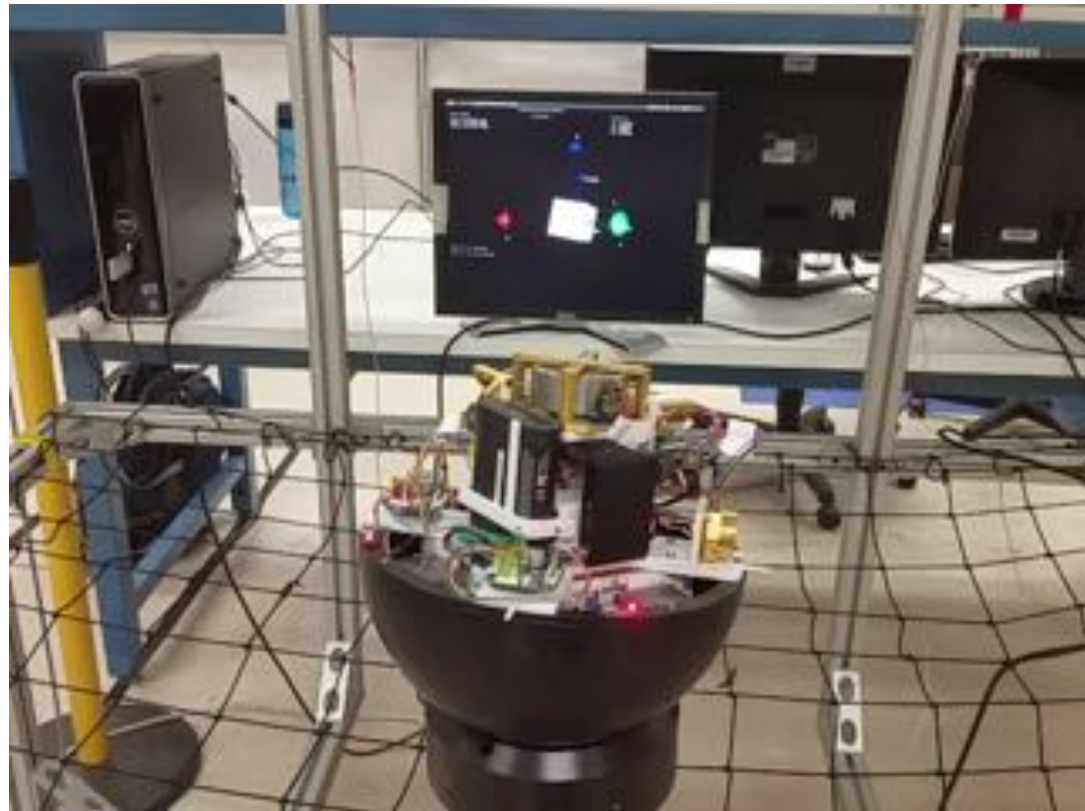
Integration with one of the following:

1. Simulink: custom modeling of S/C + MB UxV + Orbit
2. AGI-STK (HPOP & Viz.)
3. Gazebo (MP / MB & Viz.)

Real-time execution on OBC
Targeted deployment for V&V onto

1. OBC on HIL S/C Simulator at SRL Lab
2. OBC on an orbiting S/C

CubeTAS test-bed for nanosat Attitude maneuvering

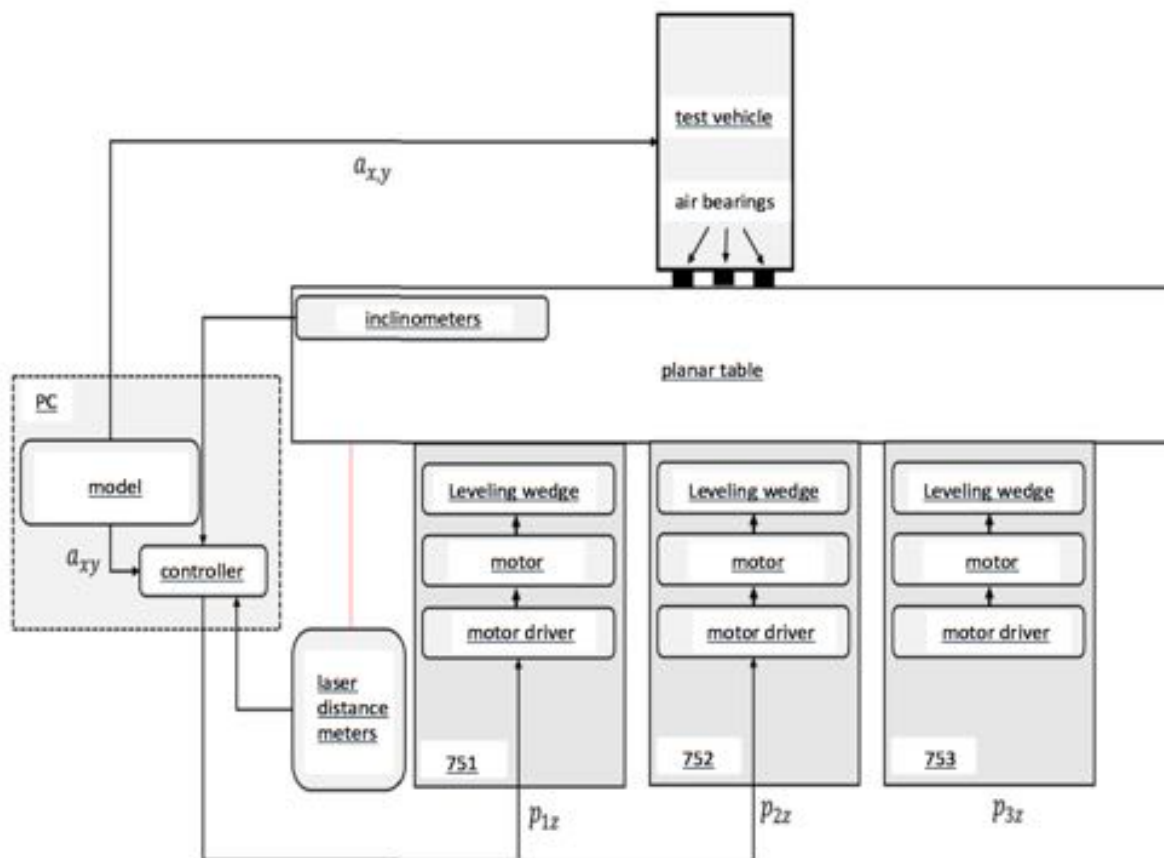


[Refs:

- 1) Chesi S., Gong Q., Pellegrini V., Cristi R., Romano M., "Automatic Mass Balancing of a Spacecraft Three-Axis Simulator: Analysis and Experimentation," *Journal of Guidance, Control, and Dynamics*, 2014.
- 2) Chesi S., Perez O., Romano M., "A Dynamic Hardware-in-the-loop Three-Axis Simulator of Nanosatellite Dimensions". *Journal of Small Satellites*. 2015.
- 3) Halis C. Polat, Josep Virgili-Llop, and Marcello Romano, Survey, *Statistical Analysis and Classification of Launched CubeSat Missions with Emphasis on the Attitude Control Method*. *Journal of Small Satellites*, 2016.
- 4) Dae Young Lee, Hyeongjun Park, Marcello Romano, and James W. Cutler, *Development and Experimental Validation of a Multi-Algorithmic Hybrid Attitude Determination and Control System for a Small Satellite*, *Aerospace Science and Technology*, 2018.
- 5) Guglielmo Cervettini, *Master Thesis*, Politecnico di Torino, 2017.]

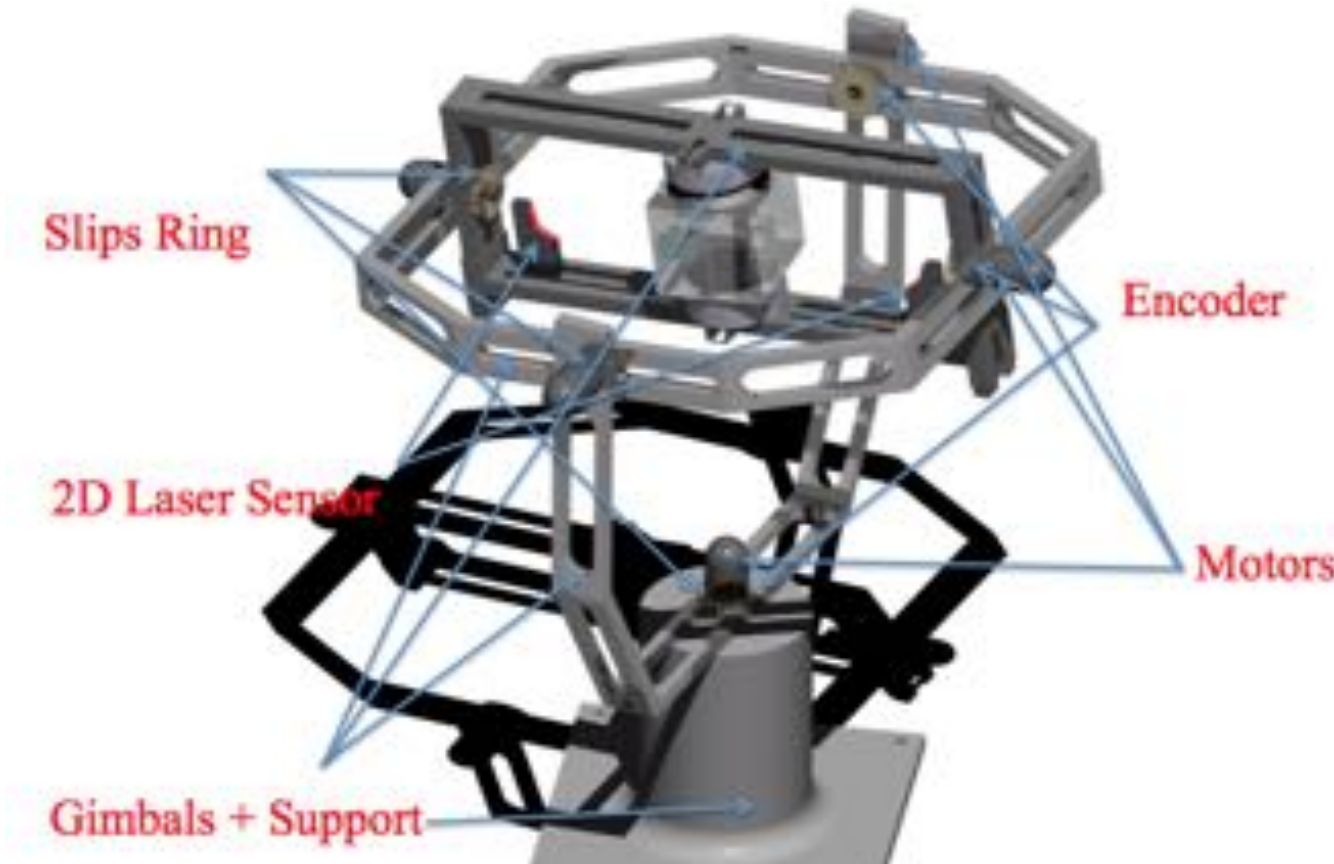
Floating S/C simulator with environmental perturbation emulation (under development)

(e.g. relative orbital dynamics or small-body gravity or “long-term maneuver” on infinite plane)



[Ref: Virgili-Llop, J., Zappulla, R., Romano, M.: Tilting table for emulation of orbital mechanics. 2017. Patent Pending.]

Concept of a 3-axis simulator with unlimited rotation



[Ref: Romano, M., Chesi S.: Angularly Unbounded Three-Axis Spacecraft Simulator, 2013. Patent Pending.
Application number US 14/908,483]

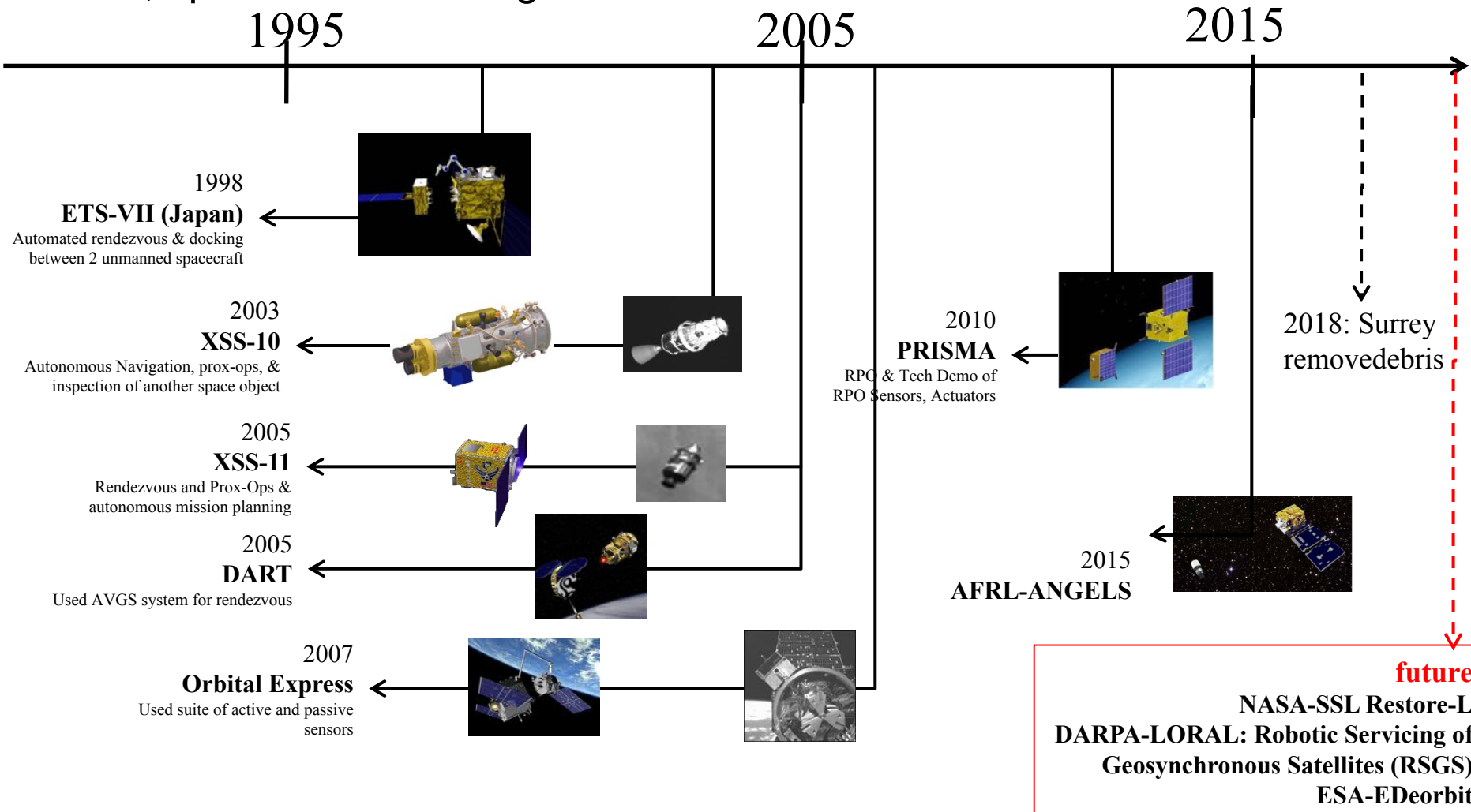
Outline of the talk

Overview of selected research topics

- 1) Spacecraft Engineering & Technology
-Development of HIL Test-beds for Spacecraft Proximity and Attitude Maneuvering (GN&C)
- 2) Orbital Robotics
-Design/test G&C Algorithms for S/C Proximity & Attitude Maneuvering
- 3) Space Flight Mechanics
-Using Residual Aero-Drag for Attitude Maneuvers
-Seeking and Using Exact Solutions of Rigid Body Motion

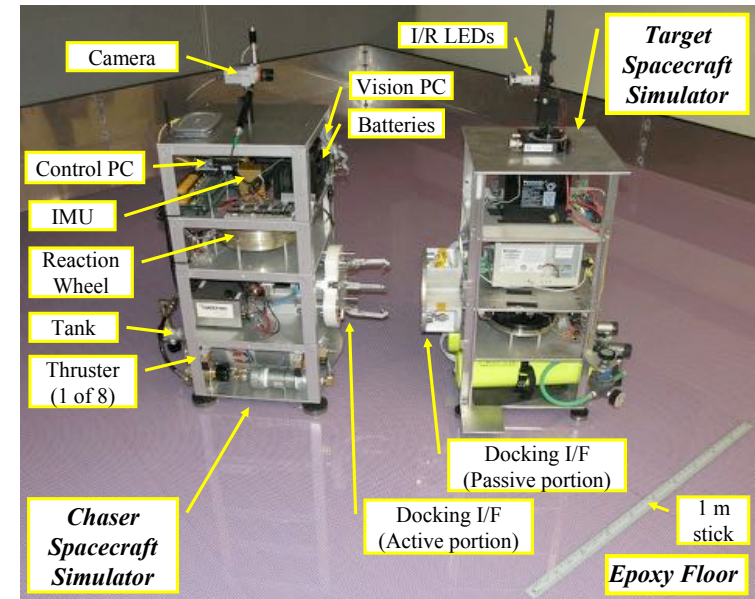
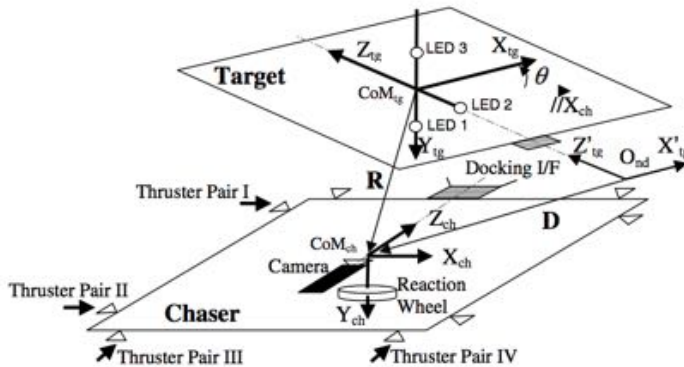
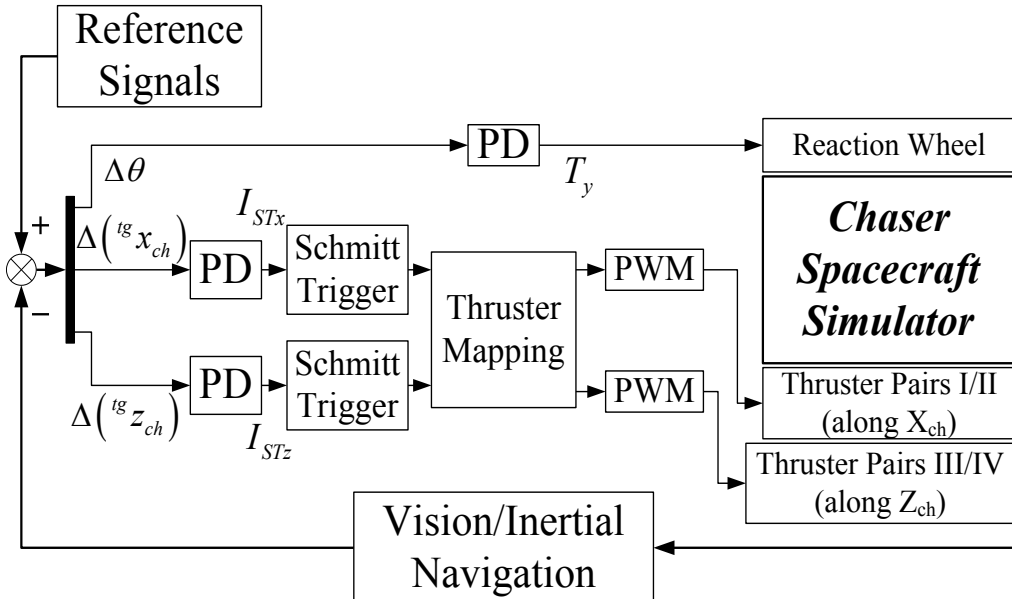
Perspective on Proximity Maneuver

S/C proximity maneuvers are of interest for several current and future space applications, including: autonomous docking, on-orbit assembly, space debris removal, spacecraft servicing.



Autonomous docking with stabilized target

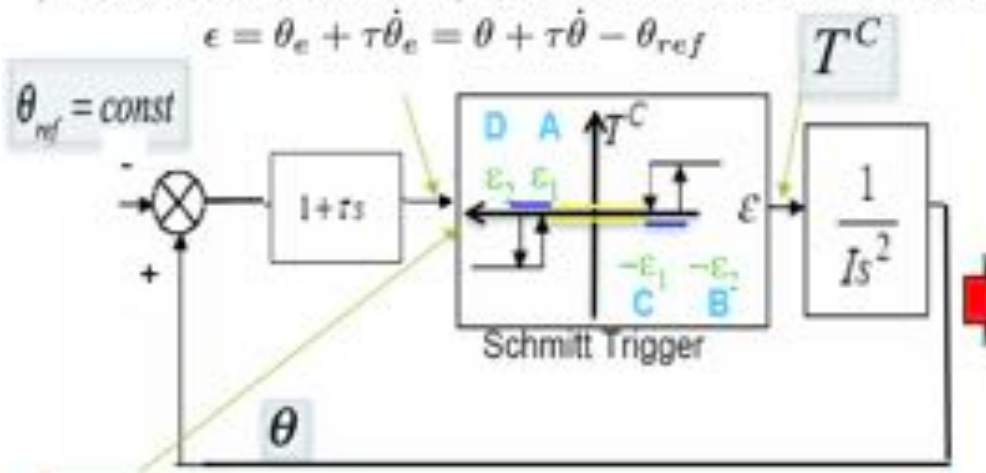
- PD + way-point path planning. Num Sim + test on NPS floor



[Ref: Romano, Friedman, Shay, *Laboratory Experimentation of Autonomous Spacecraft Approach and Docking to a Collaborative Target*, AIAA Journal of Spacecraft and Rockets, 2007]

PD thruster control logic with Schmidt Trigger block (dead zone + hysteresis) [SISO**]

We want to allow limited excursion of angle and angle rate: this method allows to get automatically a bang-off-bang Control and to avoid chattering near the target state, where a "desired-size" limit cycle is achieved
 (Values of maximum acceptable attitude and attitude rate errors are given by mission requirements.)



"unusual" positive axis direction convention used here to comply with convention in literature on Schmidt trigger

= dead zone
 = hysteresis

ϵ = control signal (combining position & rate error)

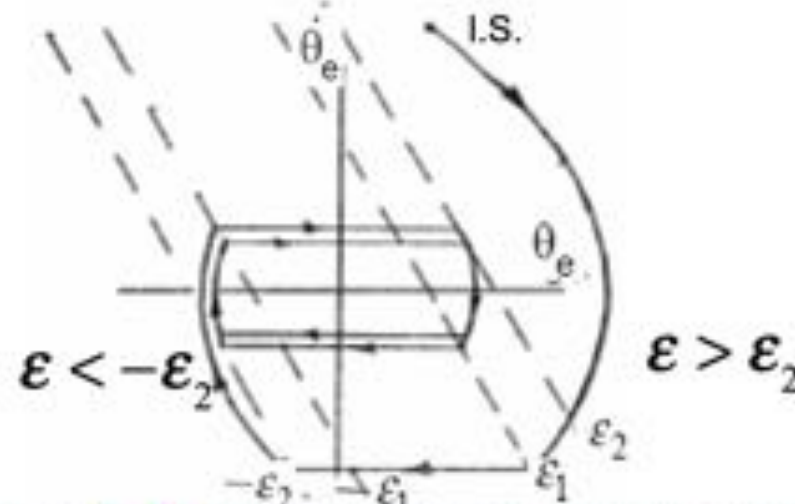
T^C = torque input to the spacecraft

(3 possible values: T_{max} , 0, $-T_{max}$)

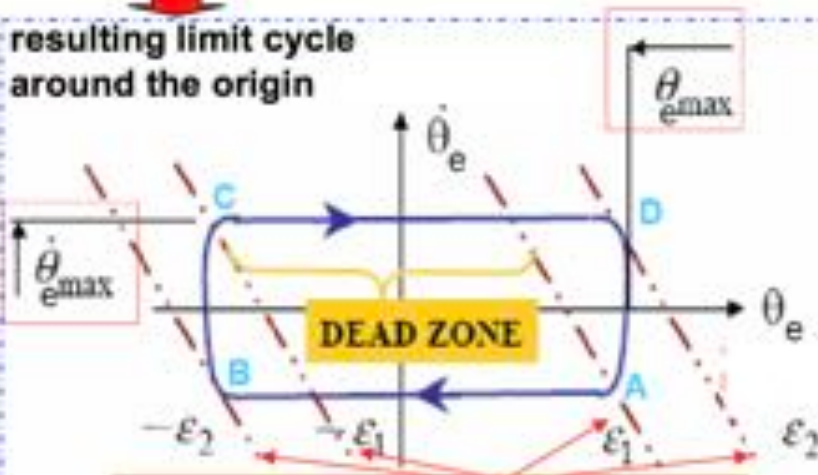
$\epsilon_1 > 0, \epsilon_2 > 0, \tau > 0$

= control parameters chosen on the basis of desired $\theta_{e_{max}}$, $\dot{\theta}_{e_{max}}$ and damping ratio (see later)

E.g. motion starting from large initial error (epsilon)



resulting limit cycle around the origin



Constant error lines (switch lines):
 $\theta_e + \tau \dot{\theta}_e = \bullet, \quad \bullet \in \{\epsilon_1, \epsilon_2, -\epsilon_1, -\epsilon_2\}$

Further references:

Kaplan pag. 262, Chobov pag. 42, Bryson's Spacecraft dynamics

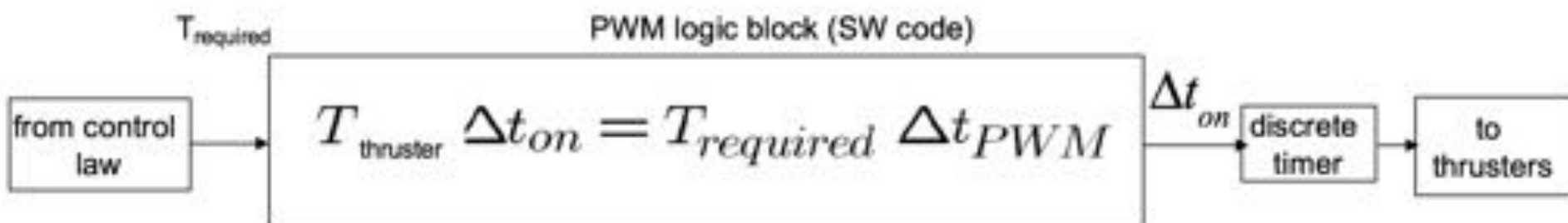
** OK for each loop of 3 axis control for small angles/angular rates

NPS-AE381B

Pulse Width Modulation

Only the pulse width is modulated. PWM is easily realized with microprocessors.

Basic principle for implementation of one-axis PWM (for more axes, PWM code has to be integrated with Thruster Mapping code):

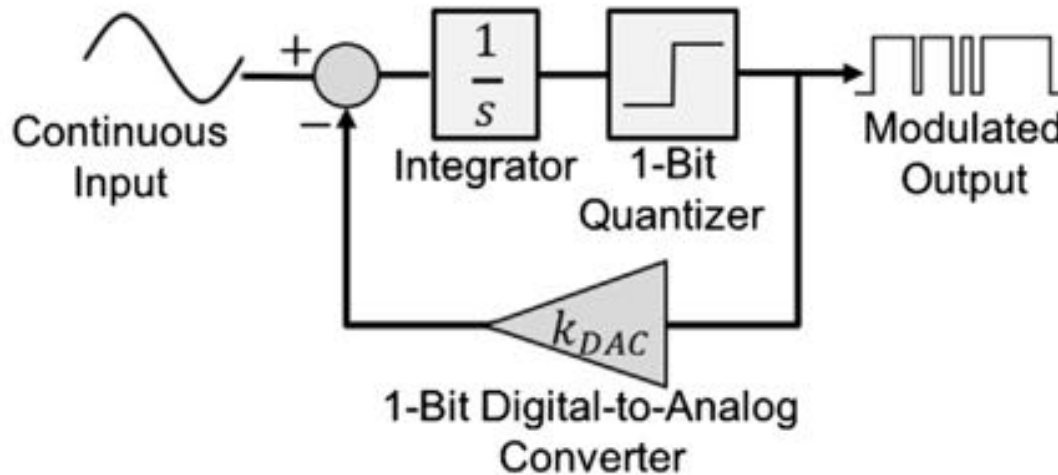


Constraints:

$$\left\{ \begin{array}{l} \Delta t_{PWM} = n_1 * \Delta t_{RTcontrol} \quad \text{e.g. } n_1 = 10 \\ \Delta t_{on} = n_2 * \Delta t_{RTcontrol} \quad n_2 = 0, 1, 2, \dots \quad n_1 \\ \Delta t_{on} > \Delta t_{min\ PW} \\ \Delta t_{PWM} \ll 1 / (\text{SystemBandwidth}) \end{array} \right.$$

Note: PWM may excite structural modes in resonance with the PWM sample time
[caution needed in choosing sample time]

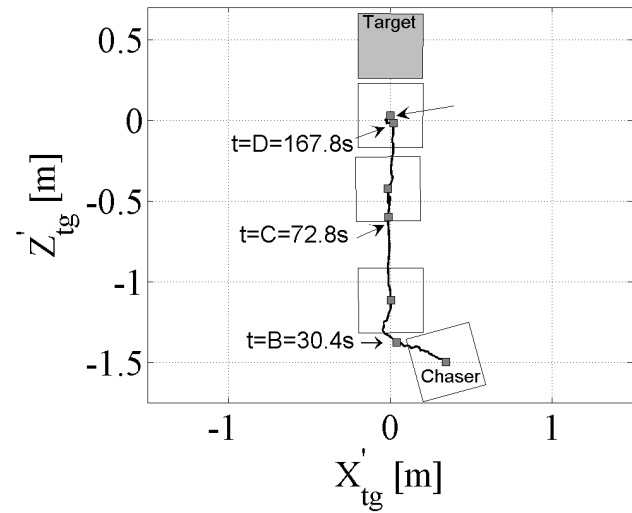
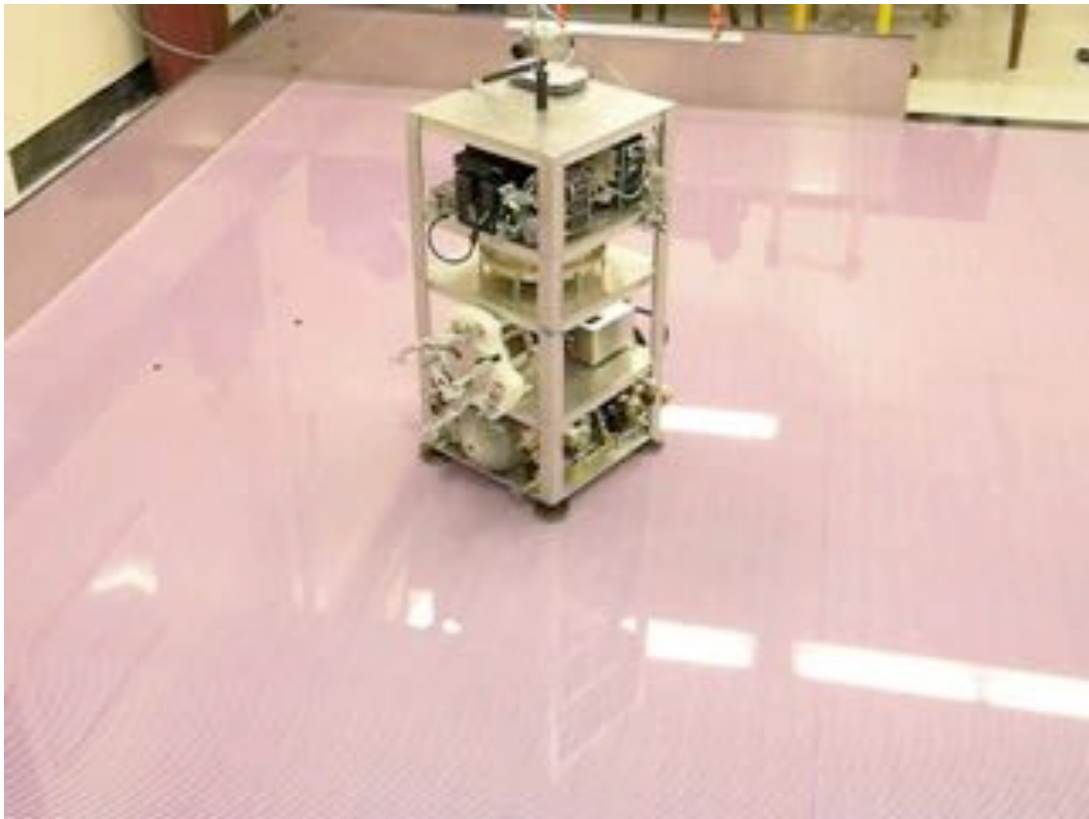
Recent development: Sigma-Delta Modulation for Thrusters' actuation



- ▶ Increased accuracy of reproduction of continuous command impulse w.r.t. PWM
- ▶ Previously spreadly used in signal processing

[Zappulla R., Virgili-Llop J., Romano M., *Spacecraft Thruster Control via Sigma-Delta Modulation. Journal of Guidance, Control, and Dynamics. 2017*]

Autonomous docking with stabilized target [ctnd]



[Ref: M. Romano, D.A. Friedman, T.J. Shay, *Laboratory Experimentation of Autonomous Spacecraft Approach and Docking to a Collaborative Target*, AIAA Journal of Spacecraft and Rockets, 2007.]

Autonomous docking with stabilized target [ctnd]

Discrete Kalman Filters implementation for the relative navigation, fusing vision and IMU data

Attitude

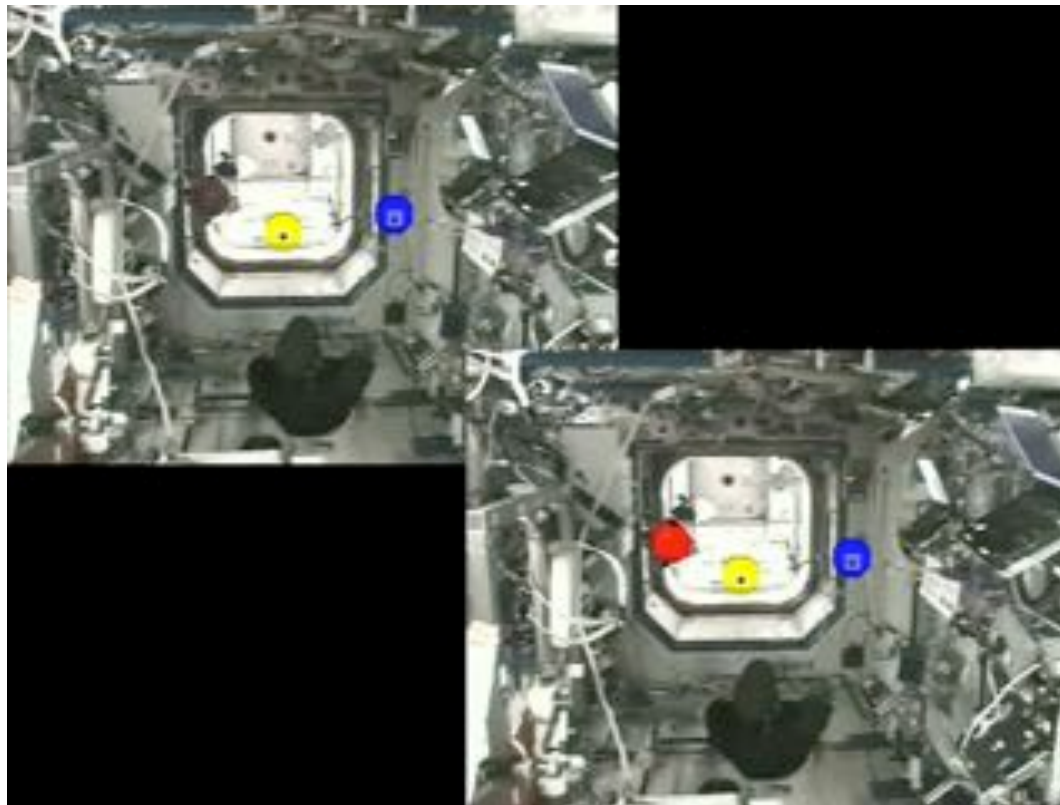
$$\left\{ \begin{array}{l} \mathbf{x}_k = [\theta_k \quad \gamma_k]^T, \quad \dot{\theta}_k = \tilde{\ddot{\theta}}_k \\ H_{[k-\text{delay}(k)]} = [1 \quad 0], \quad \mathbf{v}_{[k-\text{delay}(k)]} = [v_{\theta \text{ cam}} [k-\text{delay}(k)]] \end{array} \right.$$

Translation

$$\left\{ \begin{array}{l} \mathbf{x}_k = [{}^{\text{tg}}x_{\text{ch } k} \quad {}^{\text{tg}}\dot{x}_{\text{ch } k} \quad \beta_{xk} \quad {}^{\text{tg}}z_{\text{ch } k} \quad {}^{\text{tg}}\dot{z}_{\text{ch } k} \quad \beta_{zk}]^T \quad \mathbf{u}_k = [\tilde{\ddot{x}}_k \quad \tilde{\ddot{z}}_k]^T \\ H_{[k-\text{delay}(k)]} = \begin{bmatrix} 1 & 0 & 0 & 0 & 0 & 0 \\ 0 & 0 & 0 & 1 & 0 & 0 \end{bmatrix}, \\ \mathbf{v}_{[k-\text{delay}(k)]} = [v_{x \text{ cam}} [k-\text{delay}(k)] \quad v_{z \text{ cam}} [k-\text{delay}(k)]] \end{array} \right.$$

Autonomous docking with stabilized target & Obstacles

- APFG / LQR. Num. Sim. + test on ISS.



[Refs:

- 1) McCamish, Romano, Nolet, Edwards, Miller, *Flight Testing of Multiple Spacecraft Control on SPHERES During Close Proximity Operations*, AIAA Journal of Spacecraft and Rockets, 2009.
- 2) McCamish, Romano, Yun, *Autonomous Distributed Control of Simultaneous Multiple Spacecraft Proximity Maneuvers*, IEEE Transactions on Automation Science and Engineering, 2010.]

Suboptimal Guidance for S/C: Inv.Dyn. in Virtual Domain

Quadratic cost of control effort over the entire maneuver (or time) is minimized subjected to boundary conditions and constraints: e.g. max forces, obstacles, cone approach to target.

Path is represented by an analytic expression of few free parameters (e.g. polynomials (translation) or quaternion Bezier curves (attitude))

By inverting the dynamics along the specified paths, this results in an NLP problem that is solved using NLP tool (e.g. SNOPT or IPOPT).

Minimize

$$J = \frac{1}{2} \int_0^{t_f} (u_x^2(t) + u_y^2(t)) dt$$
$$x(\tau) = \sum_{i=0}^{n_x} a_i \tau^i \quad y(\tau) = \sum_{i=0}^{n_y} b_i \tau^i$$
$$t_\xi(\tau) = \sum_{i=1}^{n_{t\xi}} d_{\xi i} \tau^i \quad \lambda_\xi(\tau) = \frac{dt_\xi}{d\tau} = \sum_{i=1}^{n_{t\xi}} i d_{\xi i} \tau^{i-1} > 0 \quad \xi = x, y$$

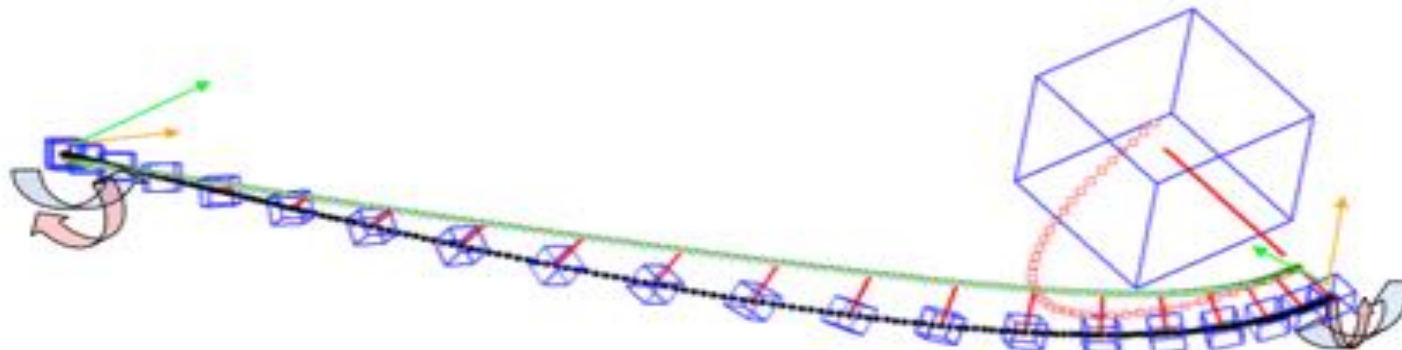
subject to:

$$t_x(\tau_f) = t_y(\tau_f), \quad t_x(\tau_f) < t_{max}$$
$$d_{\xi i} > 0 \rightarrow \lambda_{x,y}(\tau) > 0$$
$$u_{x,y}(\tau) < u_{max}$$
$$\sqrt{(x - x_{obs})^2 + (y - y_{obs})^2} > r_{obs}$$
$$\text{atan2}(x, y) - \alpha_{cone \text{ orient.}} < \alpha_{half \text{ cone}}$$

[Ref:

Yakimenko, Direct Method for Rapid Prototyping of Near Optimal Aircraft Trajectories, J. of Guidance, Control, and Dynamics, 2000.]

IDVD for S/C Maneuver: simulation results



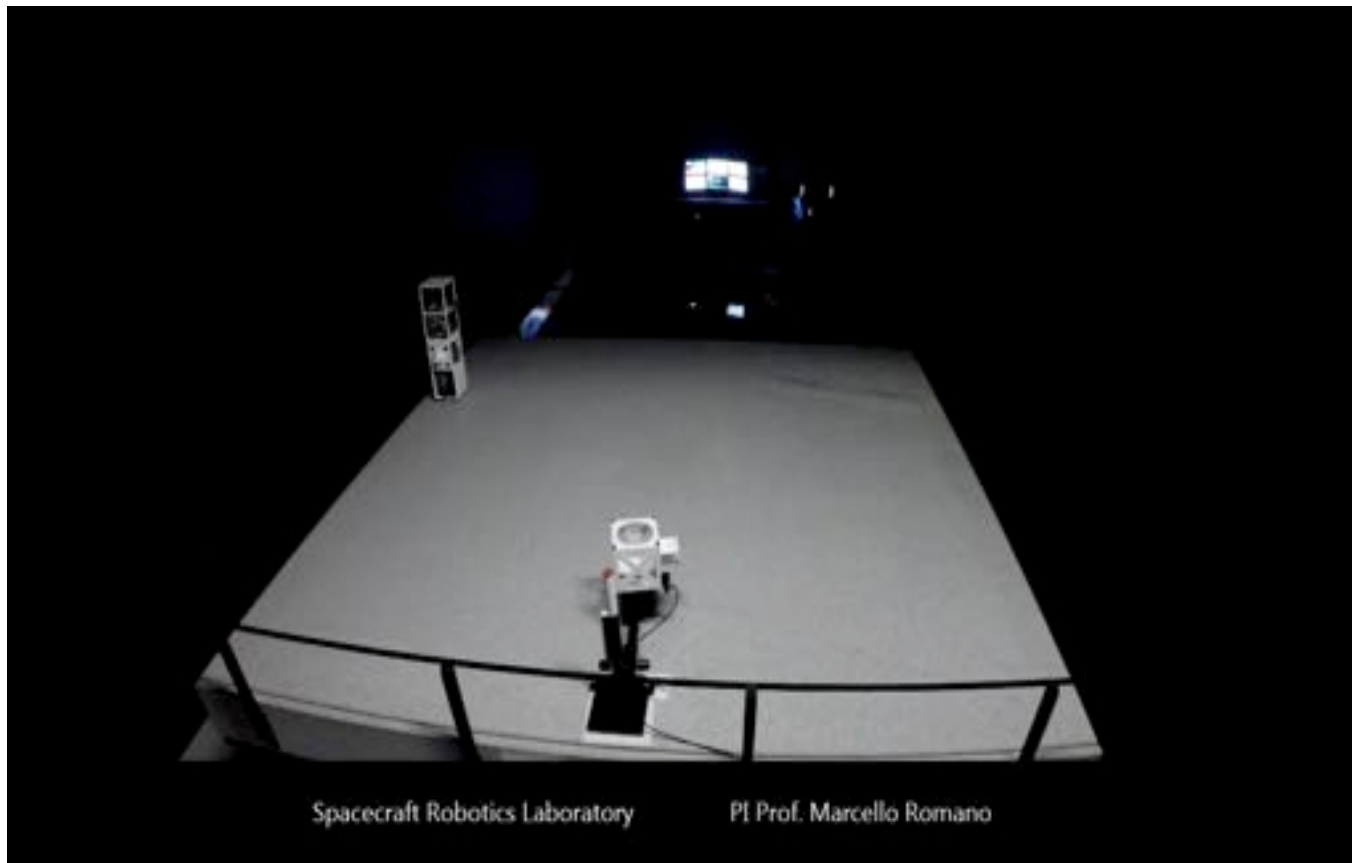
- ▶ Numerical simulations results (IDVD+SNOPT with comparison to PS)
 - ◆ Guidance of a spacecraft approaching a tumbling object
 - Boyarko, Yakimenko, Romano, *Optimal Rendezvous Trajectories of a Controlled Spacecraft and a Tumbling Object*, *J. of Guidance, Control, and Dynamics*, 2011
 - Ventura, Ciarcia', Romano., Walter, *A fast and near-optimal guidance for docking to uncontrolled target*. *J. of Guidance, Control, and Dynamics*, 2017.
 - ◆ Time-optimal reorientation of a spacecraft
 - Boyarko, Romano, Yakimenko. *Time-Optimal Reorientation of a Spacecraft Using an Inverse Dynamics Optimization Method*, *J. of Guidance, Control, and Dynamics*, 2011.
 - Ventura, Romano, Walter, *Performance Evaluation of the Inverse Dynamics Method for Optimal Spacecraft Reorientation*, *Acta Astronautica*, 2015.

IDVD for S/C Maneuver: experimental results

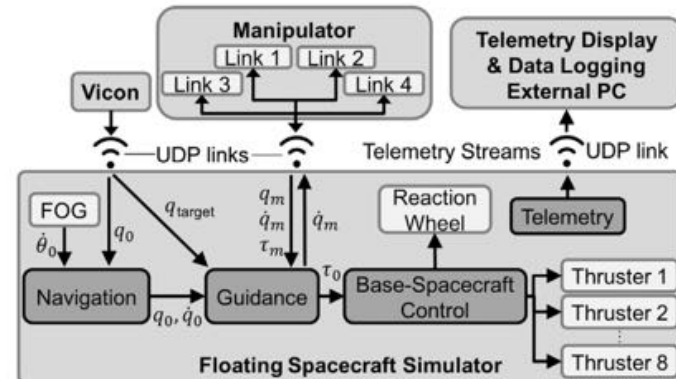
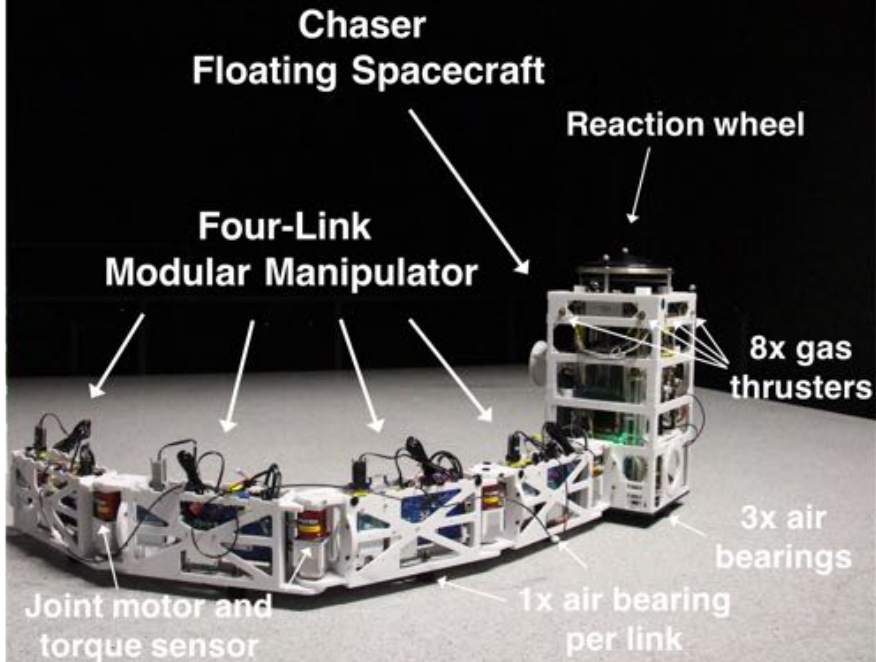
- ▶ Real-time implementation and tests on POSEYDIN air-bearing table

- ◆ Docking with rotating target (ID+SGRA)

--Wilde M., Ciarcia' M., Grompone, A., Romano M., *Experimental Characterization of Inverse Dyn. Guidance & Control in Docking with a Rotating Target*, J. of Guid., Control, and Dynamics, 2016.



MANISAT: S/C + Manipulator Test-bed



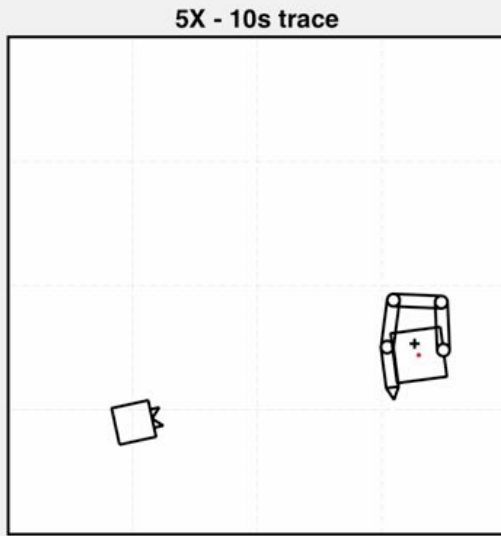
Parameter	Value
Mass	13 kg
Inertia	0.28 kg m ²
Dimensions (length × width)	0.27 × 0.27 m
Force per thruster	~0.15 N (inlet pressure dependent)
Reaction wheel model	Ball Aerospace RW-2.5-A1
Reaction wheel max. angular momentum	±2.5 N m s
Reaction wheel mean max. torque	±53.2 m N m
Air tank capacity	1.868 cm ³ (14 ci)
Air tank nominal pressure	20.7 MPa (3000 psi)
Air bearings & thrusters nominal inlet pressure	413.7 Pa (60 psi)
Onboard CPU	Intel® Atom™ 1.6 GHz Z530 processor with 2 GB of RAM
Real-time operating System	Linux 2.6 with the RT_PREEMPT patch [47]
FOG	KVH® DSP-3000
Test bed residual linear acceleration \ddot{r}	~1.871 × 10 ⁻⁴ m/s ² (or ~19.1 µg)
Test bed residual angular acceleration $\ddot{\theta}$	~7.56 × 10 ⁻² deg/s ²

Selected manipulator parameters.

Parameter	Value
Mass per link	2.9 kg
Inertia per link	≈0.0364 kg m ²
Docking interface mass	0.2 kg
Last link's inertia	≈0.0385 kg m ²
Link's length (axis-to-axis)	0.38 m
Link's width	0.08 m
Motor max. torque	±1.8 N m
Absolute encoder resolution	150°
Torque sensor range	±2 N m
Max. joint angular displacement	± 90°
Control and telemetry rate	50 Hz

base/manipulator ratios
 mass: ~1 (typically >>1)
 inertia: ~1/50 (typically <<1)

S/C + robotic manipulator capturing a rotating target



(Telemetry animation)

Chaser:

- Phase 1 - Initial approach (free-flying): LQR control with thrusters and RW to 1st hold position.
- Phase 2 - Manipulator unfold (free-floating): the base reacts to the manipulator's motion
- Phase 3 - Final approach (free-flying): LQR control with thrusters and RW (updated inertia) reaching a second hold state (tracking a circle centered at target CoM).
- Phase 4 – Capture (free-floating): manipulator extends.

Target:

Actuated by thrusters with tracking control of position & attitude.

[Ref:

Virgili-Llop, Zappulla, Drew , Romano Laboratory Experiments of Resident Space Object Capture by a Spacecraft-Manipulator System. Aerospace Science and Technology. 2017.]

Marcello Romano, mromano@nps.edu

Equations of motion

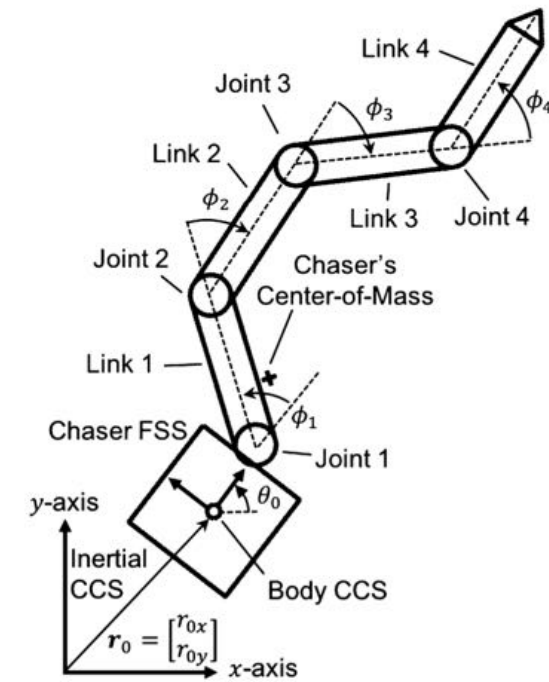
The equations of motion of a robotic multibody system with a moving base can be written as in Eq. (1), with \mathbf{H} denoting the generalized inertia matrix, \mathbf{C} the generalized convective inertia matrix (Coriolis and centrifugal forces), and $\boldsymbol{\tau}$ the generalized forces acting on the system. The vector \mathbf{q} denotes the generalized variables of the system, representing a convenient set of variables that fully describe the state of the multibody system. The generalized forces $\boldsymbol{\tau}$ are the forces that act upon these generalized variables \mathbf{q} .

$$\mathbf{H}(\mathbf{q})\ddot{\mathbf{q}} + \mathbf{C}(\mathbf{q}, \dot{\mathbf{q}})\dot{\mathbf{q}} = \boldsymbol{\tau} \quad (1)$$

The generalized variables \mathbf{q} can be decomposed $\mathbf{q} = [\mathbf{q}_0 \mathbf{q}_m]^T$ into base-spacecraft variables \mathbf{q}_0 , containing the position and orientation of the base, and manipulator related variables \mathbf{q}_m , containing the manipulator's joint angular displacements. Using this decomposition, the equations of motion can be expanded as shown in Eq. (2). The generalized forces can also be decomposed $\boldsymbol{\tau} = [\boldsymbol{\tau}_0 \boldsymbol{\tau}_m]^T$ into base-spacecraft forces and torques $\boldsymbol{\tau}_0$ and torques acting on the manipulator joints $\boldsymbol{\tau}_m$.

$$\begin{bmatrix} \mathbf{H}_0 & \mathbf{H}_{0m} \\ \mathbf{H}_{0m}^T & \mathbf{H}_m \end{bmatrix} \begin{bmatrix} \ddot{\mathbf{q}}_0 \\ \ddot{\mathbf{q}}_m \end{bmatrix} + \begin{bmatrix} \mathbf{C}_0 & \mathbf{C}_{0m} \\ \mathbf{C}_{m0} & \mathbf{C}_m \end{bmatrix} \begin{bmatrix} \dot{\mathbf{q}}_0 \\ \dot{\mathbf{q}}_m \end{bmatrix} = \begin{bmatrix} \boldsymbol{\tau}_0 \\ \boldsymbol{\tau}_m \end{bmatrix} \quad (2)$$

The \mathbf{H}_{0m} term conveys the dynamic coupling of the system. Numerically large values in the elements of \mathbf{H}_{0m} reveal a strong dynamic coupling between the base and the manipulator.



$$\mathbf{q}_0 = \begin{bmatrix} r_{0x} \\ r_{0y} \\ \theta_0 \end{bmatrix} \quad \boldsymbol{\tau}_0 = \begin{bmatrix} F_{0x} \\ F_{0y} \\ n_0 \end{bmatrix}$$

$$\mathbf{q}_m = \begin{bmatrix} \phi_1 \\ \phi_2 \\ \phi_3 \\ \phi_4 \end{bmatrix} \quad \boldsymbol{\tau}_m = \begin{bmatrix} n_1 \\ n_2 \\ n_3 \\ n_4 \end{bmatrix}$$

[Ref: Virgili-Llop, Zappulla, Drew , Romano Laboratory Experiments of Resident Space Object Capture by a Spacecraft-Manipulator System. Aerospace Science and Technology. 2017.]

Control Algorithm

Phase 1 & 3: approach

The LQR controller determines the forces and torques to be imparted on the base-spacecraft τ_0 . The manipulator joints are commanded to hold their state ($\dot{q}_m = \ddot{q}_m = 0$). To formulate the LQR, a state-space representation of the system's dynamics is required.

$$\dot{x} = Ax + Bu \quad (6a)$$

$$x = \begin{bmatrix} q_0 \\ \dot{q}_0 \end{bmatrix} \quad (6b)$$

$$u = \tau_0 \quad (6c)$$

The state matrix A and input matrix B defined, using Eq. (2), as follows:

$$A = \begin{bmatrix} \mathbf{0}_{3 \times 3} & I_{3 \times 3} \\ \mathbf{0}_{3 \times 3} & -H_0^{-1}C_0 \end{bmatrix} \quad (7a)$$

$$B = \begin{bmatrix} \mathbf{0}_{3 \times 3} \\ H_0^{-1} \end{bmatrix} \quad (7b)$$

where $I_{3 \times 3}$ and $\mathbf{0}_{3 \times 3}$ denote a 3×3 identity and zero matrix, respectively.

During these maneuvers, the manipulator configuration remains constant, making the inertia matrix H_0 a constant. In contrast, the convective inertia matrix is a function of the base-spacecraft angular velocity $C_0 = f(\dot{q}_0)$ and is not constant. As defined, the system is in effect nonlinear. A State-Dependent Riccati Equation (SDRE) technique could be used to design a nonlinear regulator [39].

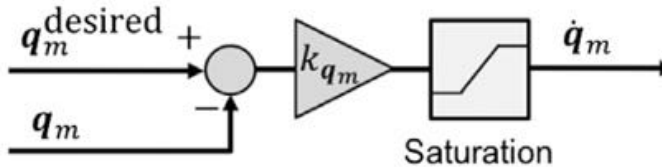
To obtain an Linear Time-Invariant (LTI) system, and simplify the design of the LQR controller, the $H_0^{-1}C_0$ term is neglected, resulting in the following simplified state matrix:

$$A \approx \begin{bmatrix} \mathbf{0}_{3 \times 3} & I_{3 \times 3} \\ \mathbf{0}_{3 \times 3} & \mathbf{0}_{3 \times 3} \end{bmatrix} \quad (8)$$

This simplification is justified because the terminal conditions of Ph.1 and Ph.3 are hold positions with zero velocities (or small velocities in the rotating target case).

$$\dot{q} \approx \mathbf{0} \implies C_{0m} \approx \mathbf{0} \quad (9)$$

Phase 2: free-floating unfold



Control Algorithm (ctnd)

Phase 4: capture (resolved-motion-rate controller)

The differential kinematic relationship can be expressed through the base and manipulator Jacobians, which map the joint space velocities of the manipulator $\dot{\mathbf{q}}_m$ and the base $\dot{\mathbf{q}}_0$, to the operational space velocities (linear and angular) of the end-effector \mathbf{t}_{EE} .

$$\mathbf{t}_{EE} = \begin{bmatrix} \dot{r}_{EEx} \\ \dot{r}_{EEx} \\ \dot{\theta}_{EE} \end{bmatrix} \quad (15a)$$

$$\mathbf{t}_{EE} = \mathbf{J}_0(\mathbf{q})\dot{\mathbf{q}}_0 + \mathbf{J}_m(\mathbf{q})\dot{\mathbf{q}}_m \quad (15b)$$

This relationship is exploited to obtain the required manipulator joint velocities $\dot{\mathbf{q}}_m$ that provide the desired end-effector motion $\mathbf{t}_{EE}^{\text{desired}}$ for a given base-spacecraft motion $\dot{\mathbf{q}}_0$.

As the vehicle operates in a planar three degrees-of-freedom environment, the manipulator's four degrees-of-freedom provide kinematic redundancy. As a result, the manipulator Jacobian \mathbf{J}_m is not square and cannot be directly inverted. The Moore-Penrose pseudoinverse \mathbf{J}_m^+ is used to obtain the solution minimizing the norm of the joint angular velocities $\dot{\mathbf{q}}_m$. This minimum-rate resolved-motion-rate controller is the one that has been implemented and takes the following form:

$$\dot{\mathbf{q}}_m = \mathbf{J}_m^+ (\mathbf{t}_{EE}^{\text{desired}} - \mathbf{J}_0 \dot{\mathbf{q}}_0) \quad (16a)$$

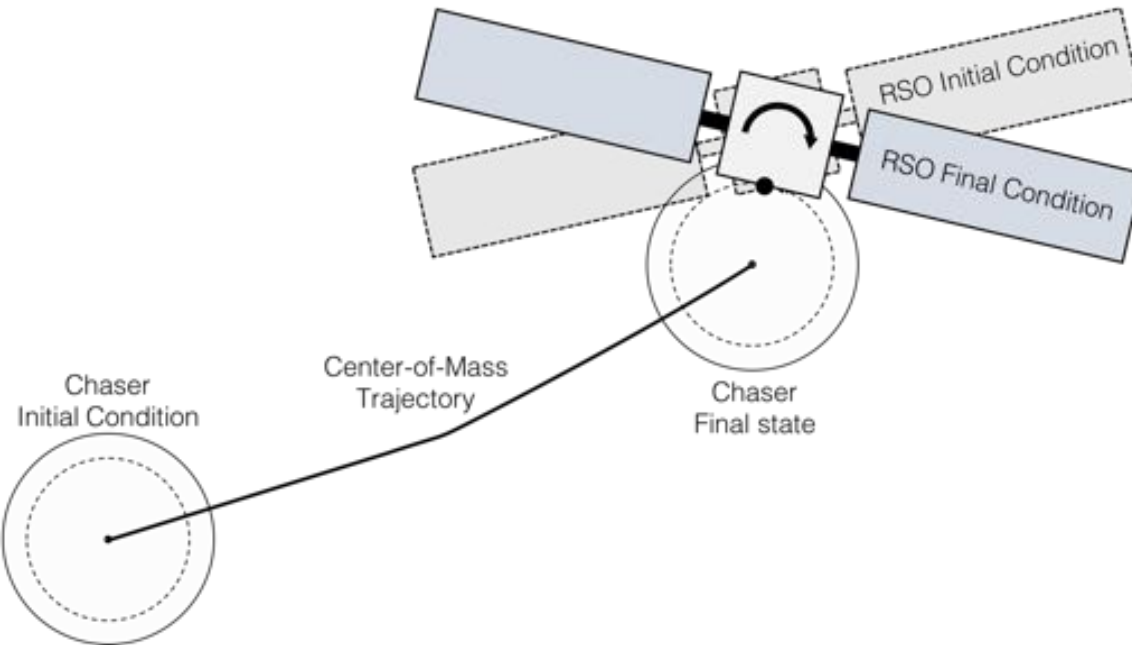
$$\mathbf{J}_m^+ = \mathbf{J}_m^T (\mathbf{J}_m \mathbf{J}_m^T)^{-1} \quad (16b)$$

The motion of the base $\dot{\mathbf{q}}_0$, required in Eq. (16) to obtain the required manipulator motion, can either be measured or predicted (e.g., using the expression in Eq. (13)). During the experimental campaign the base motion $\dot{\mathbf{q}}_0$ is determined by the onboard navigation filter.

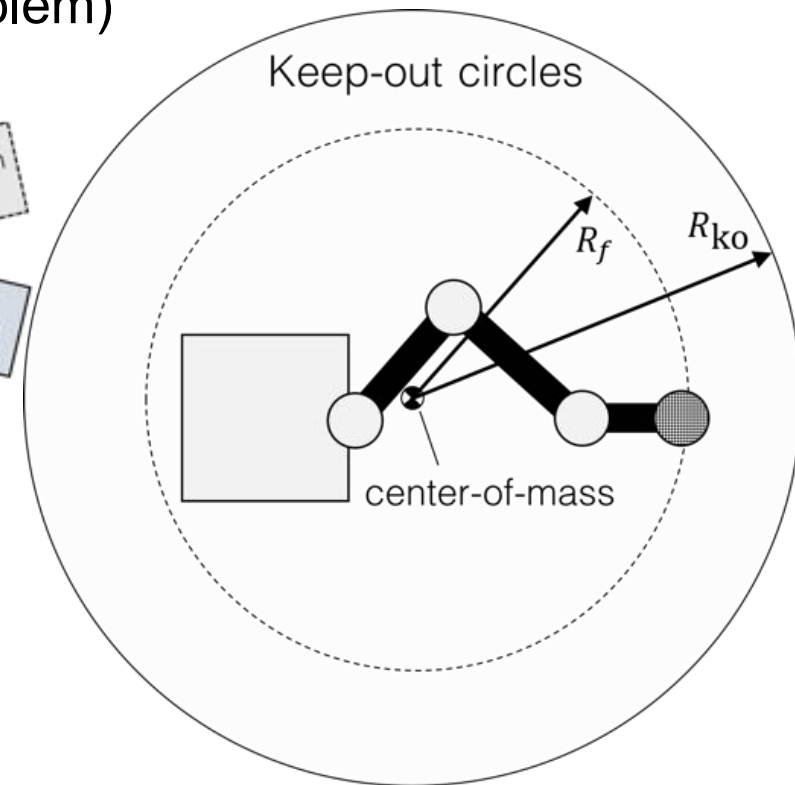
[Ref: Virgili-Llop, Zappulla, Drew , Romano Laboratory Experiments of Resident Space Object Capture by a Spacecraft-Manipulator System. Aerospace Science and Technology. 2017.]

S/C + manipulator capturing a rotating object w/t obstacle

Proposed approach: divide maneuver in two sub-maneuvers, and solve each of them as an iterative convex programming problem (with convexification of the obstacle avoidance problem)



**Step 1 – System-wide translation
(Linear Momentum)**



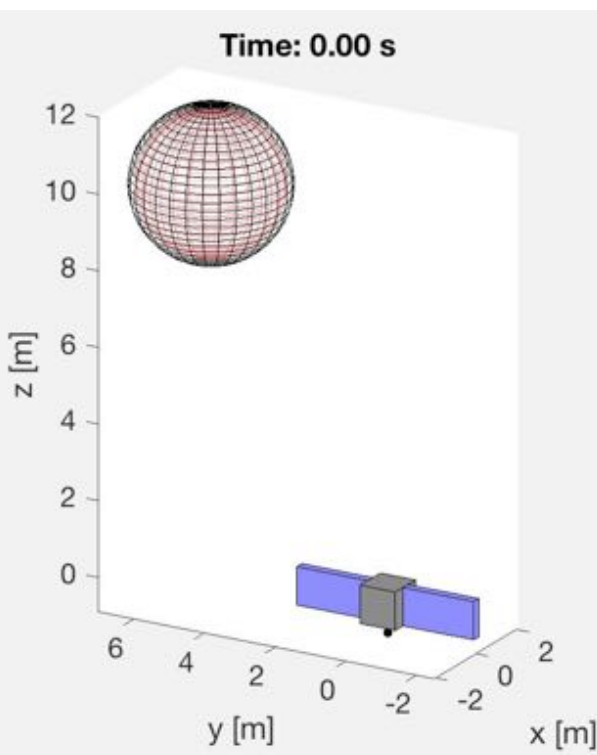
**Step 2 – Internal re-configuration
(Angular Momentum)**

J. Virgili-Llop, C. Zagaris, R. Zappulla II, A. Bradstreet, and M. Romano, "Convex optimization for proximity maneuvering of a spacecraft with a robotic manipulator," *27th AAS/AIAA Space Flight Mechanics Meeting, San Antonio, Texas, 5-9 February 2017*, 2017.

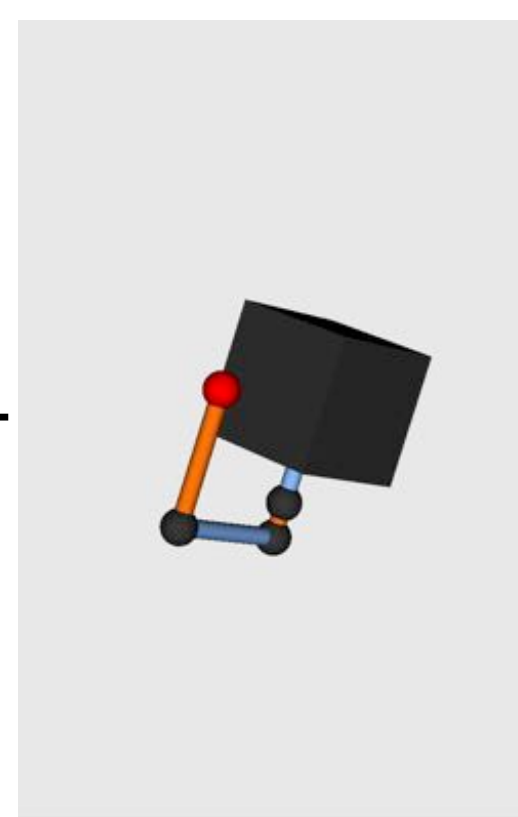
S/C/manipulator capturing a rotating object with obstacle [II]

Results of Numerical Simulations for 3D motion (& MC analysis)

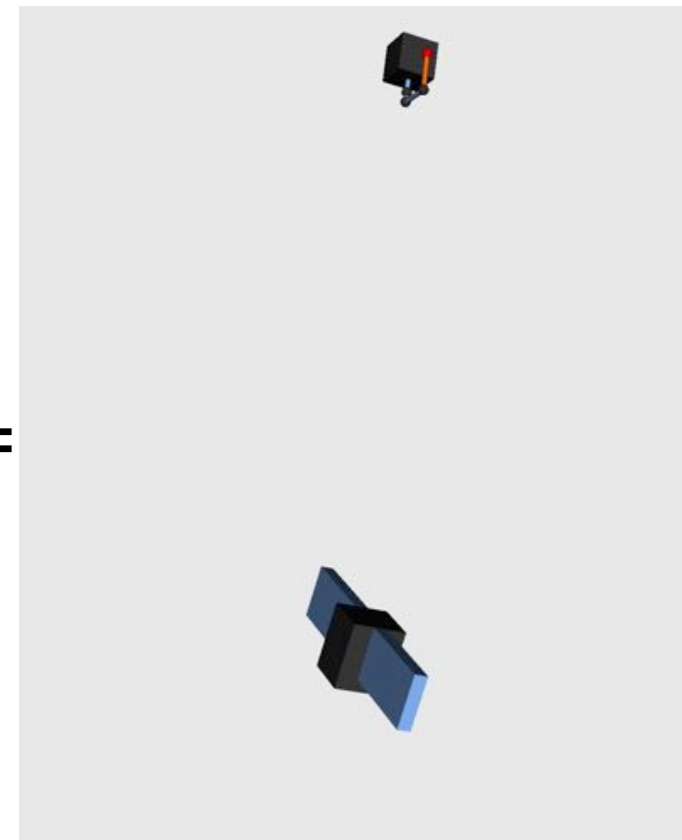
Step 1:
System-Wide Translation



Step 2:
Internal re-configuration



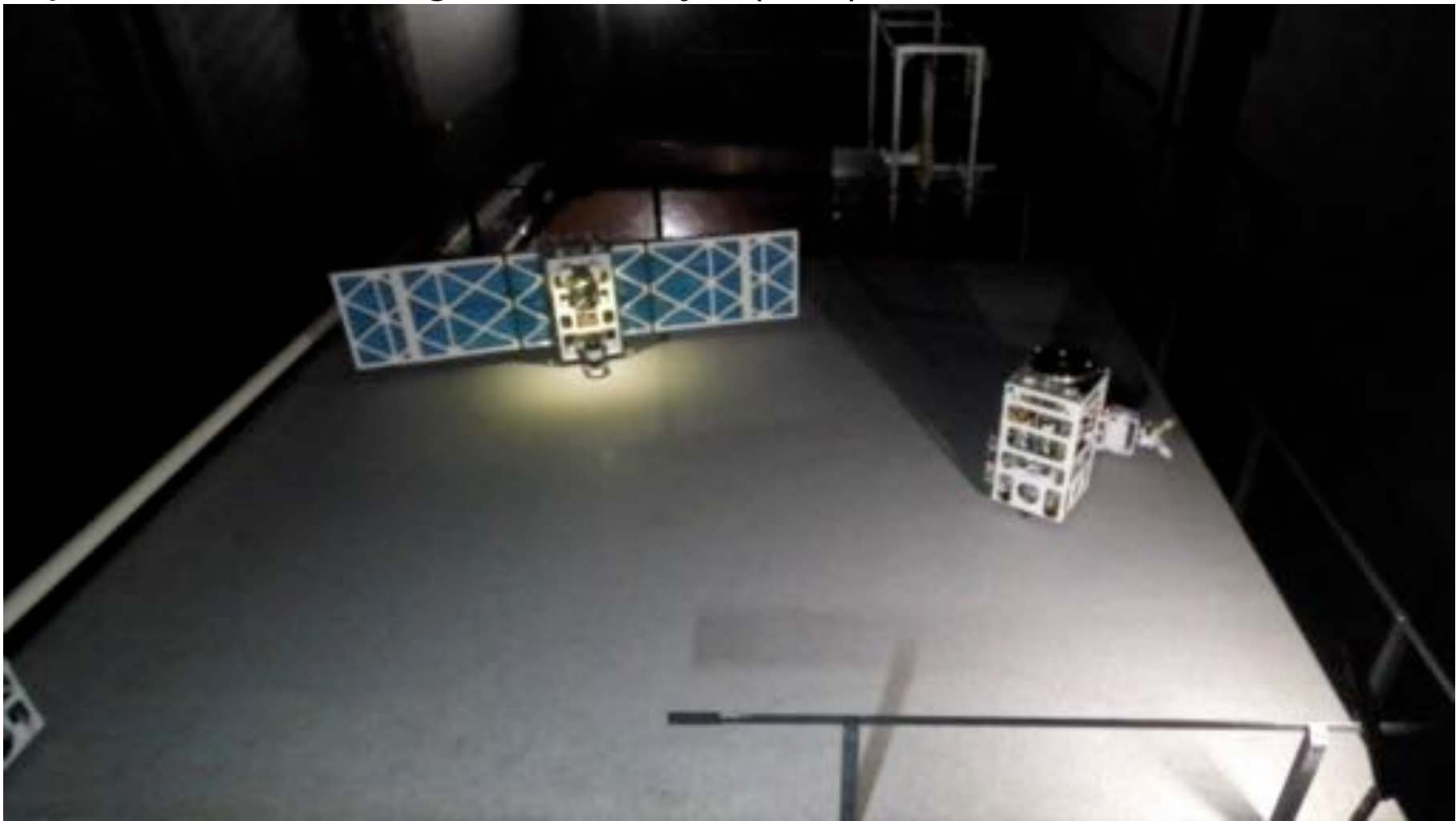
Combined Maneuver



J. Virgili-Llop, C. Zagaris, R. Zappulla II, A. Bradstreet, and M. Romano, "Convex optimization for proximity maneuvering of a spacecraft with a robotic manipulator," *27th AAS/AIAA Space Flight Mechanics Meeting, San Antonio, Texas, 5-9 February 2017*.

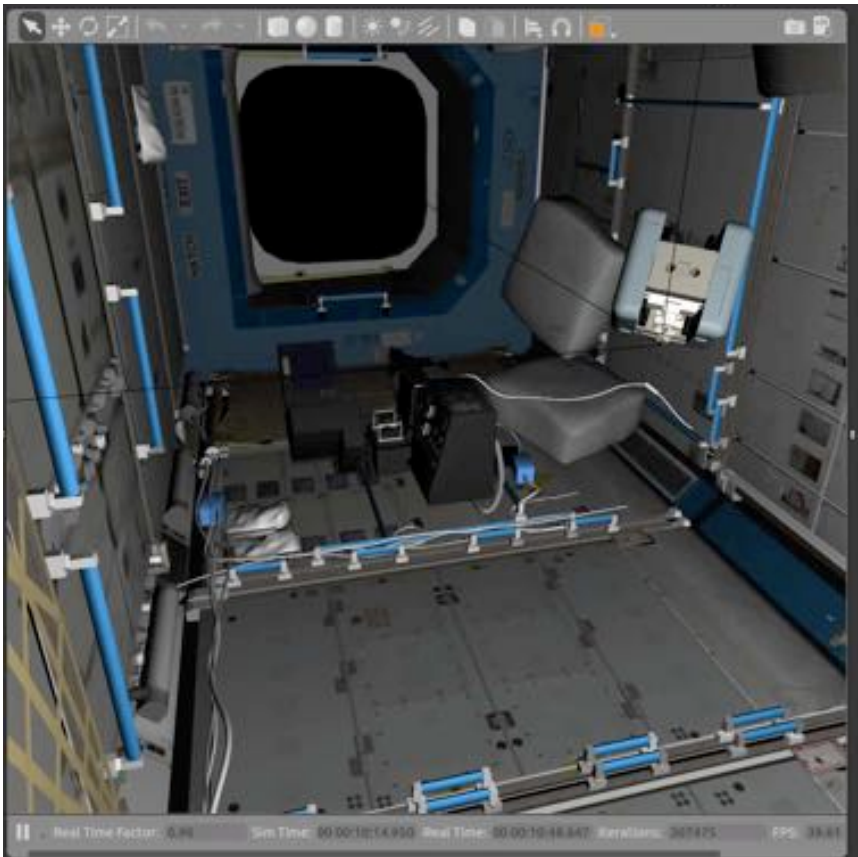
S/C/manipulator capturing a rotating object with obstacle [III]

Experimental testing in Poseidyn (10x)



J. Virgili-Llop, C. Zagaris, R. Zappulla II, A. Bradstreet, and M. Romano, "Laboratory Experiments on the Capture of a Tumbling Object by a Spacecraft-Manipulator System Using a Convex-Programming-Based Guidance," *International Journal of Robotic Research*, to appear.

Recent Developments (Fall 2017 – Spring 2018)



Dynamics/GN&C Simulation
of Astrobee on ISS Maneuver using
Simulink/ROS/Gazebo
NPS-SRL/NASA-AMES-IRL
(planned orbital test 2019)



Experimental test of GN&C
for MB-S/C Hopping Maneuver
NPS-SRL

Outline of the talk

Overview of selected research topics

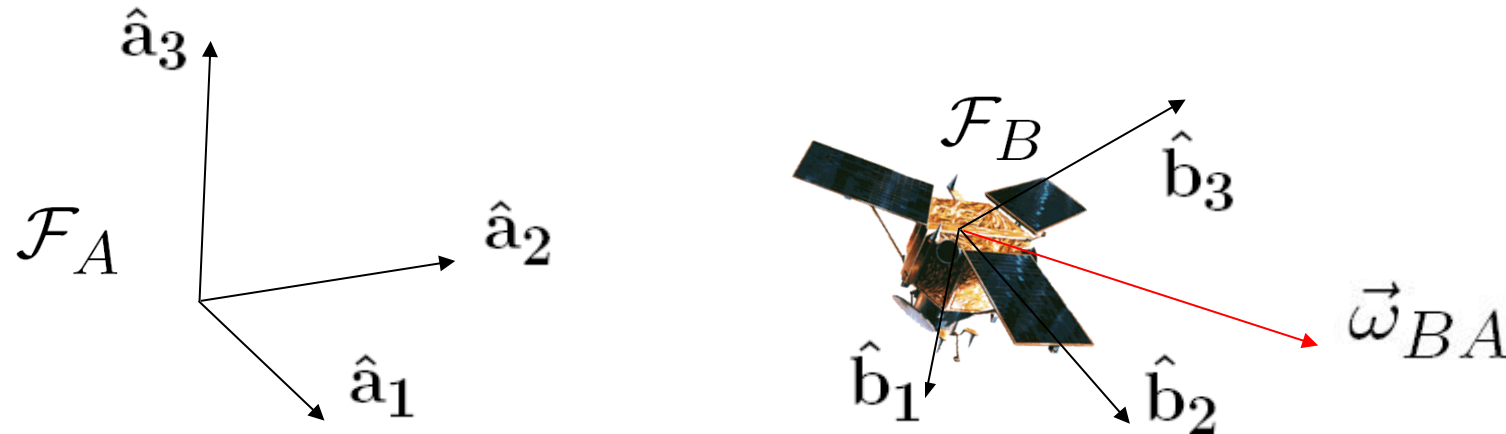
- 1) Spacecraft Engineering & Technology
-Development of HIL Test-beds for Spacecraft Proximity and Attitude Maneuvering (GN&C)
- 2) Orbital Robotics
-Design/test G&C Algorithms for S/C Proximity Maneuvering
- 3) Space Flight Mechanics
-Using Residual Aero-Drag for Attitude Maneuvers
-Seeking & Using Exact Solutions of Rigid Body Motion

Facts about Rotational Mechanics of a Rigid Body

First-order model of a spacecraft to study its rotational motion: **Rigid Body** subjected to environmental torques (for LEO satellite mainly residual atmospheric drag moment, for GEO satellite mainly solar pressure) and actuation torques.

Fundamental “peculiarities” of the rotational motion:

- 1) Large rotation do not commute → the orientation is NOT a vector.



- 2) The angular velocity is not the time derivative of a vector.

$$\vec{\omega}_{BA} \quad :| \quad \dot{C}_{BA} = -\omega_{BA}^{\times} C_{BA}$$

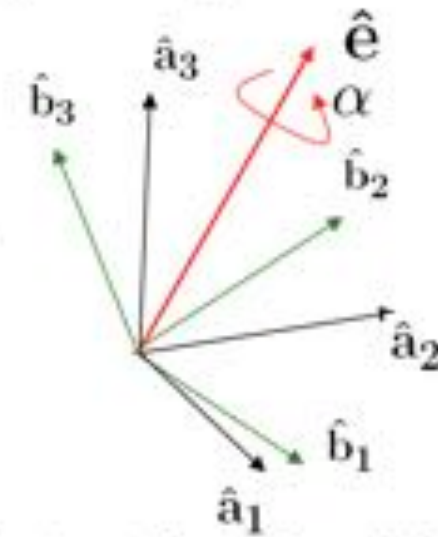
$$\omega_{BA}^{\times} \triangleq \begin{bmatrix} 0 & -\omega_z & \omega_y \\ \omega_z & 0 & -\omega_x \\ -\omega_y & \omega_x & 0 \end{bmatrix}$$

- 3) The angular momentum is not (in general) parallel to the angular velocity.

Therefore also: the orientation of a triad B relative to a triad A can be specified by specifying the Euler's axis (or principal axis) and the Euler's angle which makes A superimposed to B (if we assume without loosing generality the fixed point to be at the coincident origins of the two triads)

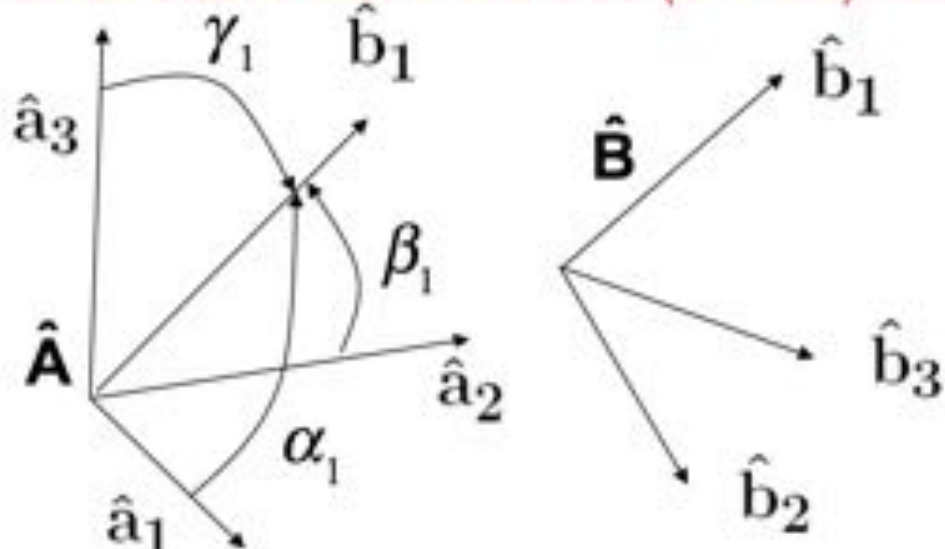
[i.e. by rotating triad A about e
of an angle alpha (or about -e by -alpha),

triad A becomes superimposed to triad B. And conversely,
by rotating about e of -alpha (or about -e of alpha)
B gets superimposed to A]



- Note 1: Euler's axis has the same scalar components along the two triads A and B
→ Mathematically: $\hat{e} = e_1 \hat{a}_1 + e_2 \hat{a}_2 + e_3 \hat{a}_3 = e_1 \hat{b}_1 + e_2 \hat{b}_2 + e_3 \hat{b}_3$
- Note 2: VERY IMPORTANT: Euler's theorem can be used to express how a RB is oriented at time t2 with respect to itself at a previous time t1. However this expression does not imply that the motion of the RB between t1 and t2 happens about the axis e (This is in general not the case!, e.g. in general e and alpha are functions of time). Similarly the displacement vector between two positions of a point mass at two different time does not imply that a straight line path of the mass.

The Direction Cosine Matrix of a CCS (or Triad) relative to another CCS (or Triad)



If:

- Two reference frames F_a and F_b are given.
- Two arbitrary Cartesian triads $\hat{\mathbf{A}}$ and $\hat{\mathbf{B}}$ are attached to F_a and F_b .

Then: the DCM C_{BA} from $\hat{\mathbf{A}}$ to $\hat{\mathbf{B}}$, or of $\hat{\mathbf{B}}$ relative to $\hat{\mathbf{A}}$, is defined as ($c = \cos$).

Scalar components of b_1 along CCS A

$$\left\{ \begin{array}{c} \hat{\mathbf{b}}_1 \\ \hat{\mathbf{b}}_2 \\ \hat{\mathbf{b}}_3 \end{array} \right\} := \left[\begin{array}{ccc} \hat{\mathbf{b}}_1 \cdot \hat{\mathbf{a}}_1 = c(\alpha_1) & \hat{\mathbf{b}}_1 \cdot \hat{\mathbf{a}}_2 = c(\beta_1) & \hat{\mathbf{b}}_1 \cdot \hat{\mathbf{a}}_3 = c(\gamma_1) \\ \hat{\mathbf{b}}_2 \cdot \hat{\mathbf{a}}_1 & \hat{\mathbf{b}}_2 \cdot \hat{\mathbf{a}}_2 & \hat{\mathbf{b}}_2 \cdot \hat{\mathbf{a}}_3 \\ \hat{\mathbf{b}}_3 \cdot \hat{\mathbf{a}}_1 & \hat{\mathbf{b}}_3 \cdot \hat{\mathbf{a}}_2 & \hat{\mathbf{b}}_3 \cdot \hat{\mathbf{a}}_3 \end{array} \right] \left\{ \begin{array}{c} \hat{\mathbf{a}}_1 \\ \hat{\mathbf{a}}_2 \\ \hat{\mathbf{a}}_3 \end{array} \right\} \quad (1)$$

Scalar components of a_1 along CCS B

which can be written in compact form as $\hat{\mathbf{B}} = C_{BA} \hat{\mathbf{A}} \leftrightarrow C_{BA} = \hat{\mathbf{B}} \cdot \hat{\mathbf{A}}^T$.
 (Notice: Wie uses the nomenclature $C^{B/A}$ for C_{BA})

- ① C_{BA} is orthonormal, i.e. $C_{BA}C_{BA}^T = E$ & $C_{BA}^T = C_{AB} = C_{BA}^{-1}$.
- ② $C_{BA}^T = \text{Adj}(C_{BA}) \rightarrow \text{Det}(C_{BA}) = 1$.
- ③ C_{BA} has one real eigenvalue (+1) and two complex conjugate eigenvalues $\exp(\pm\alpha i)$, where α is the rotation angle from $\hat{\mathbf{A}}$ to $\hat{\mathbf{B}}$.

Because of the satisfaction of Property 1 & Property 2 $\rightarrow C_{BA} \in SO(3)$

The DCM C_{BA} by definition expresses the orientation of Triad B relative to Triad A. In other words it is one of the possible orientation-parameter sets.

In particular, the DCM is the only orientation-parameter set which univocally expresses the orientation between two Triads [...stated without demonstration]. In other words, there is an *isomorphism* (1-1 correspondence) between the physical orientation of Triad B relative to Triad A and the corresponding DCM C_{BA} .

- Principal rotations are 3 planar rotations around the 3 axes of a Cartesian Coordinate System

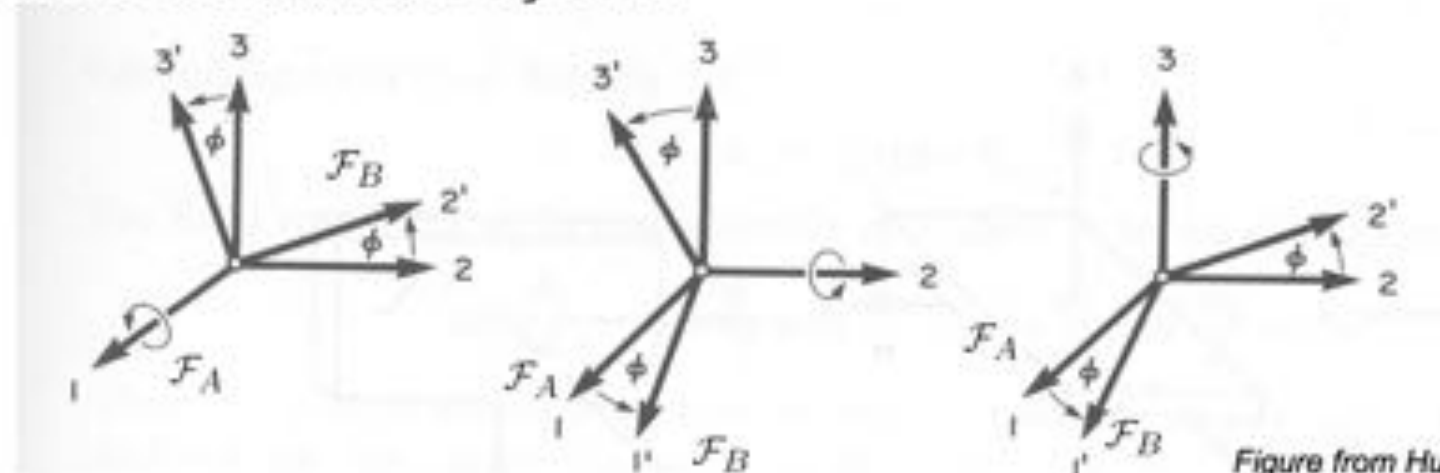


Figure from Hughes pag. 15

- DCMs corresponding to principal rotations:

$$C_1(\phi) = C_{BA} = \begin{bmatrix} 1 & 0 & 0 \\ 0 & \cos(\phi) & \sin(\phi) \\ 0 & -\sin(\phi) & \cos(\phi) \end{bmatrix}$$

$$C_2(\phi) = C_{BA} = \begin{bmatrix} \cos(\phi) & 0 & -\sin(\phi) \\ 0 & 1 & 0 \\ \sin(\phi) & 0 & \cos(\phi) \end{bmatrix}$$

$$C_3(\phi) = C_{BA} = \begin{bmatrix} \cos(\phi) & \sin(\phi) & 0 \\ -\sin(\phi) & \cos(\phi) & 0 \\ 0 & 0 & 1 \end{bmatrix}$$

Exercise:

Demonstrate these relationships by using the definition of DCM and the figures above.

They can be obtained from Euler's formula as well!

Basic Ideas:

1. a general angular displacement has three degrees of freedom
2. each principal rotation has one degree of freedom



to represent the attitude of a triad B relative to A: considering a triad D coincident with triad A, then combine a sequence of three successive principal (\rightarrow planar) rotations of the triad D in order to get it coincident with B

There are 12 possible sequence of Euler Angles:

Successive rotations around different rotated axes 123, 312, 231, 321, 213, 132

Successive rotations with first and third rotation around the same rotated axis:

121, 131, 212, 232, 313, 323

IMPORTANT POINTS:

- 1 For the same physical attitude of B relative to A, each of the twelve sequences gives different values of the three Euler's Angles
- 2 For practical use: a rotation sequence is chosen and then used consistently!

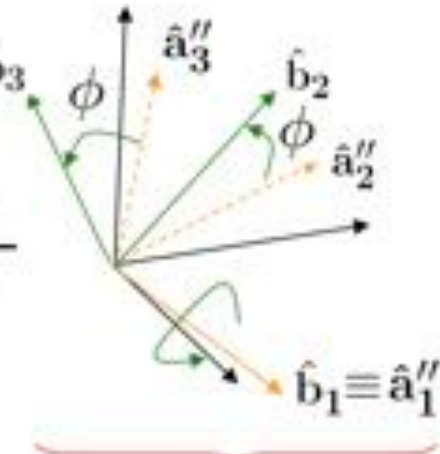
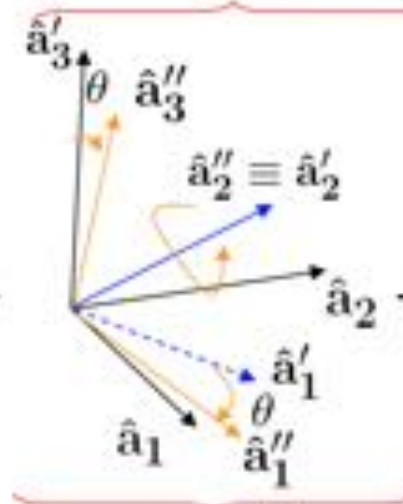
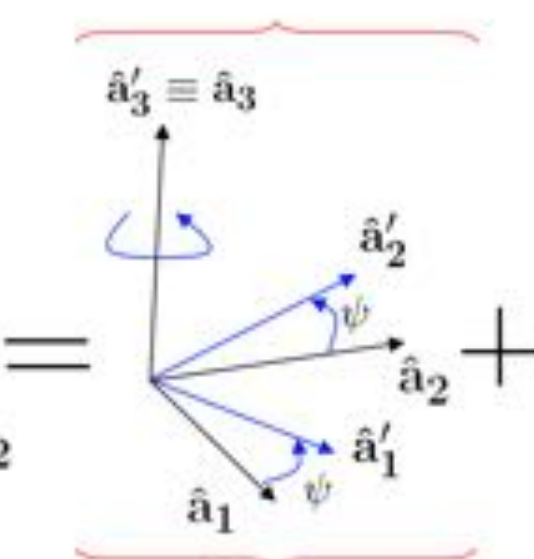
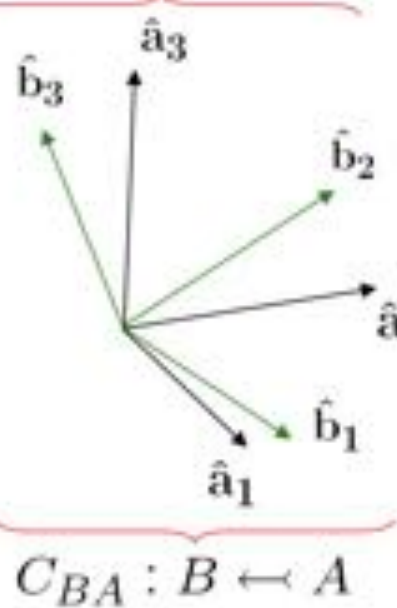
How to describe the orientation of triad B relative to A using a sequence (321) of three principal rotations?

Euler Angles Sequence 321 (often used for S/C orientation)

First: rotate from A to A' around axis 3 of A

Second: rotate from A' to A'' around the once displaced axis 2

Third: rotate from A'' to B around the twice displaced axis 1 coincident with axis 1 of B



By using the successive rotations rule:

$$C_{BA} = C_1(\phi) C_2(\theta) C_3(\psi)$$

By using the expressions of the principal rotations:

$$C_{BA} = C_1(\phi) C_2(\theta) C_3(\psi)$$



$$C_{BA} = \begin{bmatrix} C\theta C\psi & C\theta S\psi & -S\theta \\ S\phi S\theta C\psi - C\phi S\psi & S\phi S\theta S\psi + C\phi C\psi & S\phi C\theta \\ C\phi S\theta C\psi + S\phi S\psi & C\phi S\theta S\psi - S\phi C\psi & C\phi C\theta \end{bmatrix}$$

[legend: $C(\cdot) = \cos(\cdot)$; $S(\cdot) = \sin(\cdot)$]

For the DCM corresponding to the other 11 Euler's Angles sequence you may compute the DCM in the same way...

- Consider the sequence 321 of Euler Angles:

$$\theta = \frac{\pi}{2} \quad \begin{array}{l} \sin(\theta) = 1 \\ \cos(\theta) = 0 \end{array}$$

$$C_{BA\ 321} = \begin{bmatrix} 0 & 0 & -1 \\ S(\psi - \phi) & C(\psi - \phi) & 0 \\ C(\psi - \phi) & -S(\psi - \phi) & 0 \end{bmatrix}$$

Then, the rotation phi and psi become associated with the same degree of freedom and the DCM obtained from the Euler Angles does not properly describe the orientation (2 of the 3 dof are lost...): this situation is called singularity. In addition to this geometric singularity there is also a singularity in the kinematic differential equation as we will see which is source of potential problems in the numerical integration (will see).

In other words, looking at slide 15, \hat{a}_1'' becomes parallel to \hat{a}_3 and the third rotation is around the same axis of the first one \rightarrow the three Euler's angle are not able anymore to describe a general orientation of the B with respect to the A frame, once theta reaches $\pi/2$

- All of the 12 Euler Angles sequences suffer from singularities. In particular:
 - FOR ASYMMETRIC SEQUENCES (e.g. 321): when the second rotation is $\pi/2$
 - FOR SYMMETRIC SEQUENCES (e.g. 313): when the second rotation is 0
(singularities are only due to the second rotation angle)

- Quaternions are very often used for S/C attitude parametrization. The definition of quaternion is:

$$q_{BA} = \begin{bmatrix} e_1 \sin\left(\frac{\alpha}{2}\right) \\ e_2 \sin\left(\frac{\alpha}{2}\right) \\ e_3 \sin\left(\frac{\alpha}{2}\right) \\ \cos\left(\frac{\alpha}{2}\right) \end{bmatrix} = \begin{bmatrix} \hat{\mathbf{e}} \sin\left(\frac{\alpha}{2}\right) \\ \cos\left(\frac{\alpha}{2}\right) \end{bmatrix} = \begin{bmatrix} \epsilon \\ \eta \end{bmatrix}$$

- A quaternion is made of four numbers with the constraint:

$$\|q_{BA}\|^2 = q_1^2 + q_2^2 + q_3^2 + q_4^2 = \epsilon^T \epsilon + \eta^2 = 1$$

- this is the equation of a four-dimensional unit sphere
- Therefore we can state that:

$$q_{BA} \in S_1^3$$



Quaternions were invented by Hamilton (Ireland 1805-1865), as a generalization of complex numbers, satisfying the multiplication rule:

$$\mathbf{i}^2 = \mathbf{j}^2 = \mathbf{k}^2 = \mathbf{ijk} = -1 \Leftrightarrow \mathbf{ij} = \mathbf{k}, \mathbf{jk} = \mathbf{i}, \mathbf{ki} = \mathbf{j}$$

There is a double covering of $\text{SO}(3)$ by quaternions,
i.e. the conversion from CBA to quaternion is not unique

$$C_{BA} \Leftrightarrow \left\{ \begin{array}{l} (\hat{\mathbf{e}}, \alpha) \\ (-\hat{\mathbf{e}}, -\alpha) \end{array} \right\} \rightarrow q_{BA} = \begin{bmatrix} \epsilon \\ \eta \end{bmatrix}$$

$$\left\{ \begin{array}{l} (\hat{\mathbf{e}}, -2\pi + \alpha) \\ (-\hat{\mathbf{e}}, -\alpha + 2\pi) \end{array} \right\} \rightarrow q'_{BA} = \begin{bmatrix} -\epsilon \\ -\eta \end{bmatrix}$$

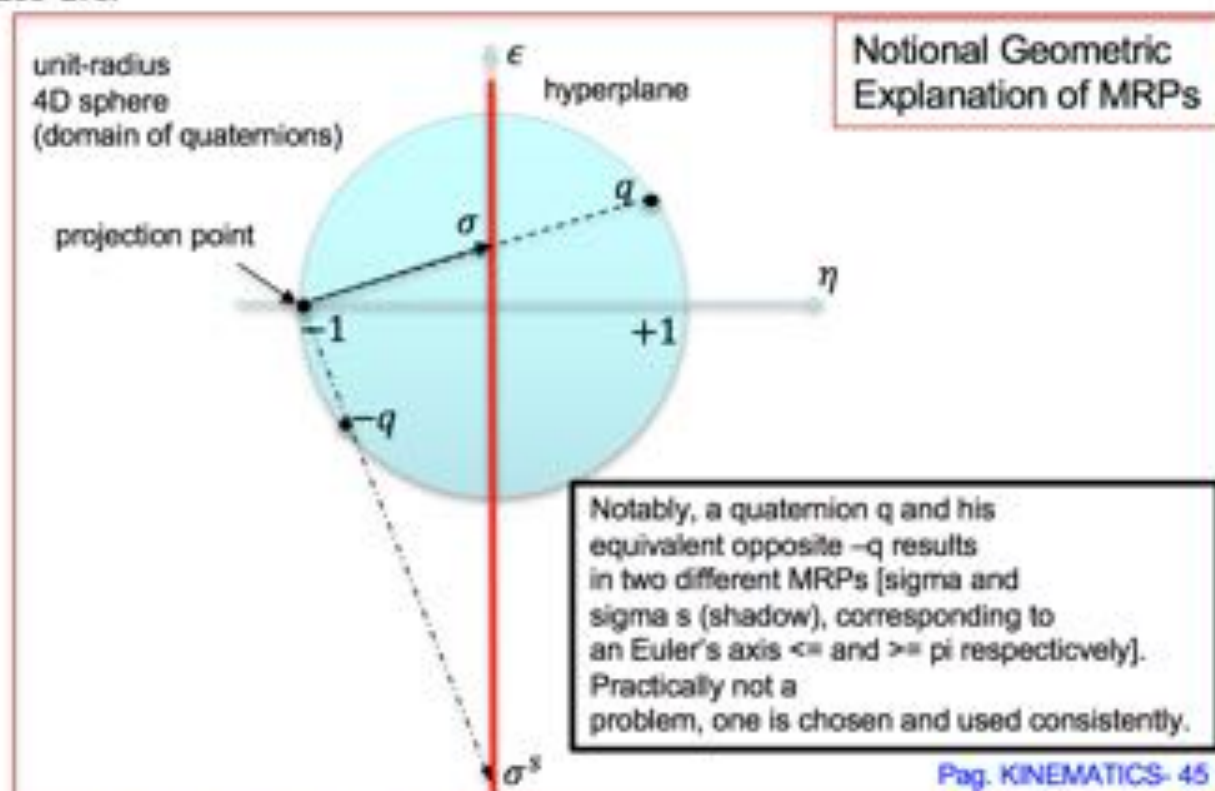
Modified Rodrigues Parameters

(minimal representation of attitude alternative to Euler's angles)

$$\sigma_i = \frac{\epsilon_i}{(1+\eta)} \quad i = 1,2,3 \leftrightarrow \sigma = \hat{e} \tan\left(\frac{\alpha}{4}\right)$$

→MRPs have a singularity for rotational displacement with Euler's angle $\alpha = \pm 2\pi$
 I.e. MRP can represent a rotational displacement up to a complete revolution (about any axis) back to the original orientation. This makes MRP a better choice than Euler's angles for a minimal representation in some S/C applications (e.g. reorientation –a.k.a. slewing– over a large angle)*.

*Ventura J., Romano M., Walter U., "Performance Evaluation of the Inverse Dynamics Method for Optimal Spacecraft Reorientation". Acta Astronautica, Volume 110, May-June 2015, Pages 266–278.

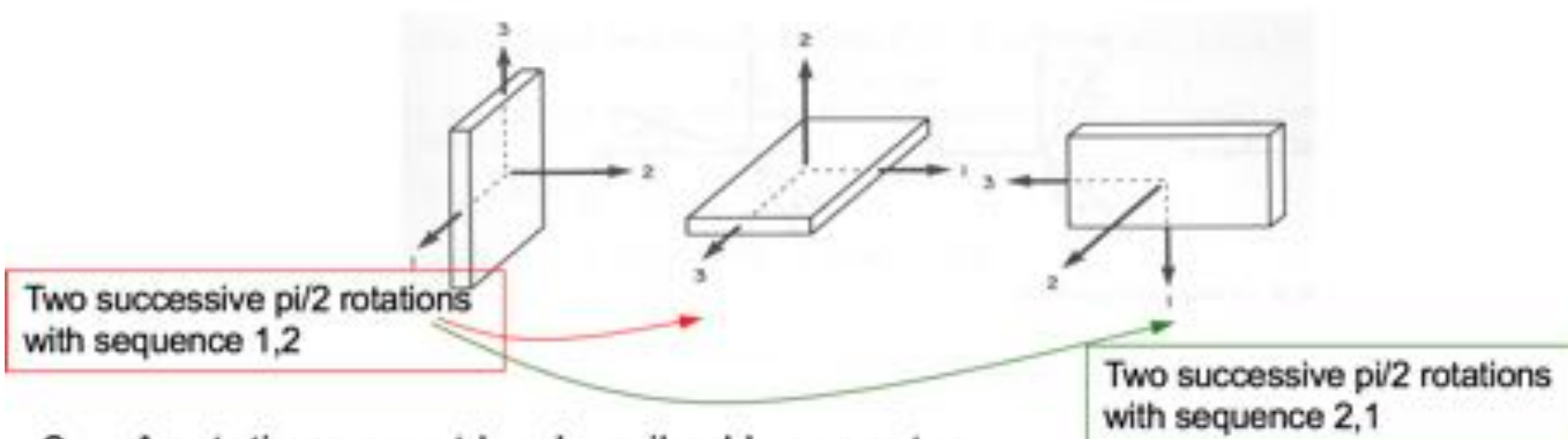


- 1. DCM
 - 2. Euler's Angles (12 sequence)
 - 3. Euler's axis and angle
 - 4. Quaternion
 - 5. Modified Rodriguez parameter
 -
 - 6. Stereographic projection
- We focus only on these ones,
as they are the most used
but there are many more

No set of three variables exists without geometric singularities (STUELPNAGEL, Siam Review, 1964)!

- DCMs, in general, do NOT commute in multiplication:

$$C_{CB} C_{BA} \neq C_{BA} C_{CB}$$



- A rotation cannot be described by a vector

1. The set of Euler Angles is not a vector...in general, summing two of them give something that does not represent the result of 2 successive rotations;
2. One could think of using $\vec{\alpha} = \alpha \hat{e}$ which would be working to represent a single orientation but, since rotations do not commute, while vectors do, summing two of these vectors $\vec{\alpha}_{BA} + \vec{\alpha}_{CB} = \vec{\alpha}_{CB} + \vec{\alpha}_{BA}$ we would obtain a third meaningless one. (not the total rotation!)

- For a generic CCS:

$$\mathbf{H}_c = \mathbf{J} \boldsymbol{\omega}_{BN}$$

$$2K = \boldsymbol{\omega}_{BN}^T \mathbf{J} \boldsymbol{\omega}_{BN}$$

- With respect to the principal CCS:

$$\mathbf{H} = \begin{Bmatrix} J_x \boldsymbol{\omega}_x \\ J_y \boldsymbol{\omega}_y \\ J_z \boldsymbol{\omega}_z \end{Bmatrix}$$

$$2K = J_x \boldsymbol{\omega}_x^2 + J_y \boldsymbol{\omega}_y^2 + J_z \boldsymbol{\omega}_z^2$$

They are the rotational equations of motion projected on the principal body fixed frame

Starting point: see slide 5.6

$$\dot{\vec{H}}_c = \vec{T}_c \longrightarrow \dot{H}_c + \boldsymbol{\omega}^{\times} H_c = T$$

- Generic body frame in the CoM

$$J_{xx}\dot{\omega}_x + J_{xy}\dot{\omega}_y + J_{xz}\dot{\omega}_z - J_{xy}\omega_x\omega_z - J_{yy}\omega_y\omega_z - J_{yz}\omega_z^2 + J_{xz}\omega_x\omega_y + J_{zz}\omega_z\omega_y + J_{yz}\omega_y^2 = T_x$$

$$J_{yx}\dot{\omega}_x + J_{yy}\dot{\omega}_y + J_{yz}\dot{\omega}_z - J_{yz}\omega_x\omega_y - J_{zz}\omega_x\omega_z - J_{xz}\omega_x^2 + J_{xx}\omega_x\omega_z + J_{xy}\omega_z\omega_y + J_{xz}\omega_z^2 = T_y$$

$$J_{zx}\dot{\omega}_x + J_{zy}\dot{\omega}_y + J_{xz}\dot{\omega}_z - J_{xz}\omega_x\omega_y - J_{yz}\omega_y\omega_z - J_{xy}\omega_z^2 + J_{yz}\omega_x\omega_y + J_{xz}\omega_z\omega_x + J_{xy}\omega_x^2 = T_z$$

- Principal axes of inertia (EULER'S EQUATIONS)

$$J_x\dot{\omega}_x + (J_z - J_y)\omega_z\omega_y = T_x$$

$$J_y\dot{\omega}_y + (J_x - J_z)\omega_x\omega_z = T_y$$

$$J_z\dot{\omega}_z + (J_y - J_x)\omega_y\omega_x = T_z$$

Using Aero-Drag for Attitude Maneuver in LEO [Concept of using shifting masses to change CoM]

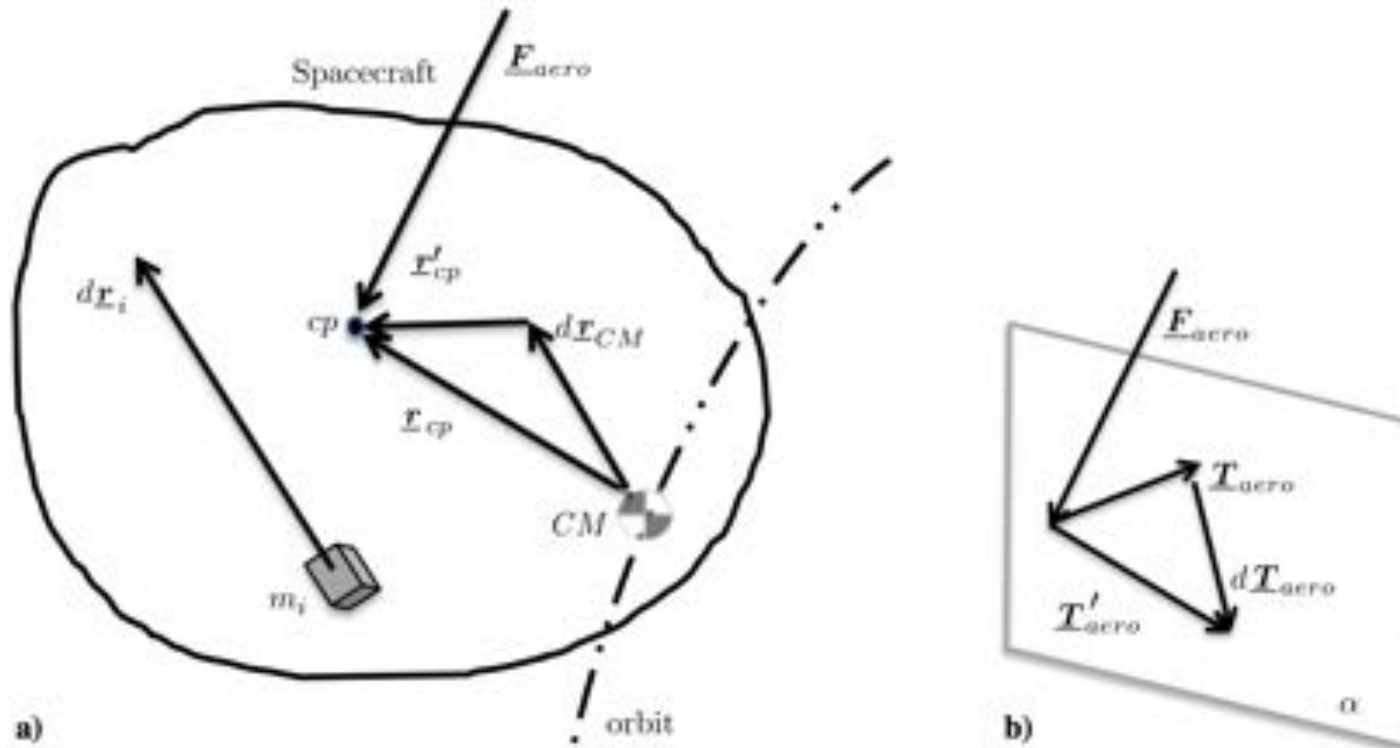
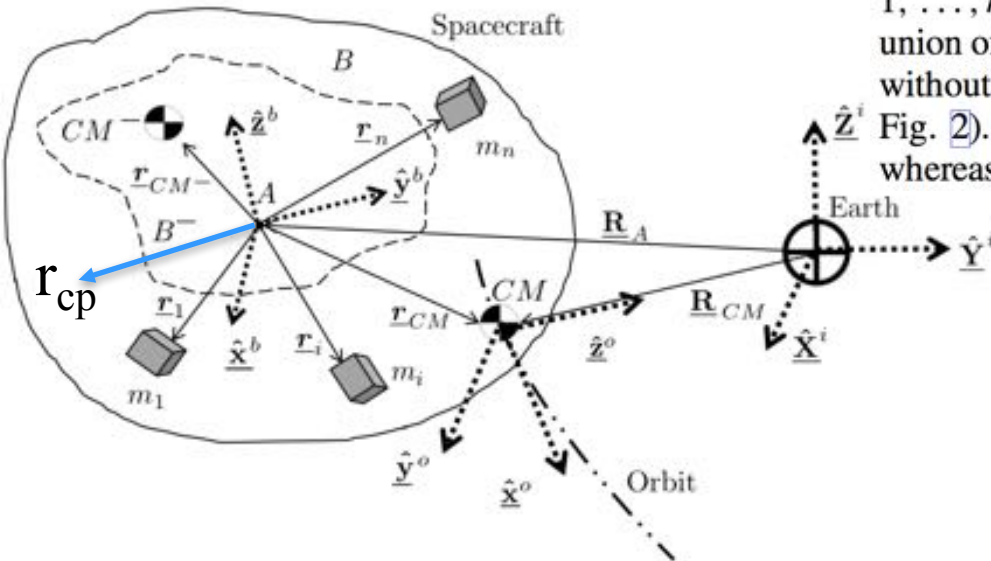


Fig. 1 Illustration of the basic concept of shifting masses on board a spacecraft in order to change the aerodynamic torque.

[Ref: Chesi, Gong, Romano, Aerodynamic Three-Axis Attitude Stabilization of a Spacecraft by Center-of-Mass Shifting. *Journal of Guidance, Dynamics and Control.* 2016]

Using Aero-Drag for Attitude Maneuver in LEO

[System model and EoM]



A spacecraft system B having n shifting masses m_i with $i = 1, \dots, n$ is considered. The spacecraft system B can be seen as the union of two portions: a body B^- encompassing the spacecraft body without the shifting masses, and the set of the n shifting masses (see Fig. 2). The center of mass of the system portion B^- is at CM^- , whereas the center of mass of the whole system B is at the CM .

$$M = M^- + \sum_{i=1}^n m_i$$

Fig. 2 Notional illustration of an orbiting spacecraft with shifting masses.

control input

$$J\dot{\omega} = -\omega^\times J\omega + \tau_{CM^-} + \tau_M + \tau_{cp}$$

$$\tau_{CM^-} = F_{\text{aero}}^\times \left(\frac{M^-}{M} \right) \mathbf{r}_{CM^-} = k_d \left(\frac{M^-}{M} \right) \left[\sum_{i=1}^p (\chi_i S_i \delta_i) \right] \hat{\nu}_{s/c}^\times \mathbf{r}_{CM^-}$$

$$k_d = -\frac{1}{2} C_D \rho \| \mathbf{v}_{s/c} \|^2, \quad \text{and} \quad \chi_i = \hat{\mathbf{n}}_i^T \hat{\mathbf{v}}_{s/c}$$

$$\tau_M = F_{\text{aero}}^\times \frac{\sum_{i=1}^n m_i \mathbf{r}_i}{M} = \frac{k_d}{M} \left[\sum_{i=1}^p (\chi_i S_i \delta_i) \right] \left(\sum_{i=1}^n m_i \mathbf{r}_i \right)^\times \hat{\nu}_{s/c}$$

$$\delta_i : \begin{cases} \delta_i = 1, & \chi_i > 0 \\ \delta_i = 0, & \chi_i \leq 0 \end{cases}$$

$$\tau_{cp} = T_{\text{aero}}^A = k_d \mathbf{r}_{cp}^\times \hat{\nu}_{s/c} \sum_{i=1}^p (\chi_i S_i \delta_i)$$

Using Aero-Drag for Attitude Maneuver in LEO [Control design (for ideal torque) using Lyapunov]

$$\boldsymbol{\tau}_{CM^-} = K_{CM^-}(-\hat{\mathbf{v}}_{s/c}^X \mathbf{r}_{CM^-}) = \Phi \Theta$$

$$K_{CM^-} = -K_d \left(\frac{M^-}{M} \right) \left[\sum_{i=1}^p (\chi_i S_i \delta_i) \right]$$

$$\Phi(\mathbf{q}_e) = -K_{CM^-} - \hat{\mathbf{v}}_{s/c}^X \quad \Theta = \mathbf{r}_{CM^-}$$

The state vector for the system can be defined as

$$\mathbf{X} = [\xi_e - 1, \boldsymbol{\eta}_e, \boldsymbol{\omega}_{bo}, \tilde{\Theta}]^T \quad (54)$$

To design the state feedback control and the adaptive law for $\hat{\Theta}$ to drive the state vector to the condition $\mathbf{X}_0 = [0, 0, 0, 0]^T$, the following Lyapunov-candidate quadratic function is used:

$$V(\mathbf{X}) = \frac{1}{2} \boldsymbol{\omega}_{bo}^T \mathbf{J} \boldsymbol{\omega}_{bo} + \frac{1}{2} \tilde{\Theta}^T \tilde{\Theta} + k_q \boldsymbol{\eta}_e^T \boldsymbol{\eta}_e + k_q (\xi_e - 1)^2 + \dots + \frac{1}{2} (K_J \boldsymbol{\omega}_{oi}^T \boldsymbol{\omega}_{oi} - \boldsymbol{\omega}_{oi}^T \mathbf{J} \boldsymbol{\omega}_{oi})$$

$$\dot{\hat{\Theta}} = \Phi^T \boldsymbol{\omega}_{bo}$$

$$\boldsymbol{\tau}_t = -\boldsymbol{\tau}_{cp} - k_q \boldsymbol{\eta}_e - k_\omega \boldsymbol{\omega}_{bo} - \Phi \hat{\Theta}$$

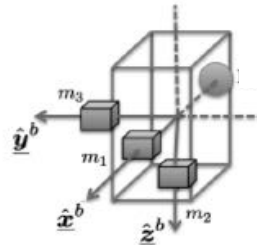
$$\lim_{t \rightarrow \infty} \boldsymbol{\omega}_{bo}(t) = 0$$

and the final attitude error can be made arbitrarily small by choosing a sufficiently large k_q .

[Ref: Chesi, Gong, Romano, Aerodynamic Three-Axis Attitude Stabilization of a Spacecraft by Center-of-Mass Shifting. *Journal of Guidance, Dynamics and Control.* 2016]

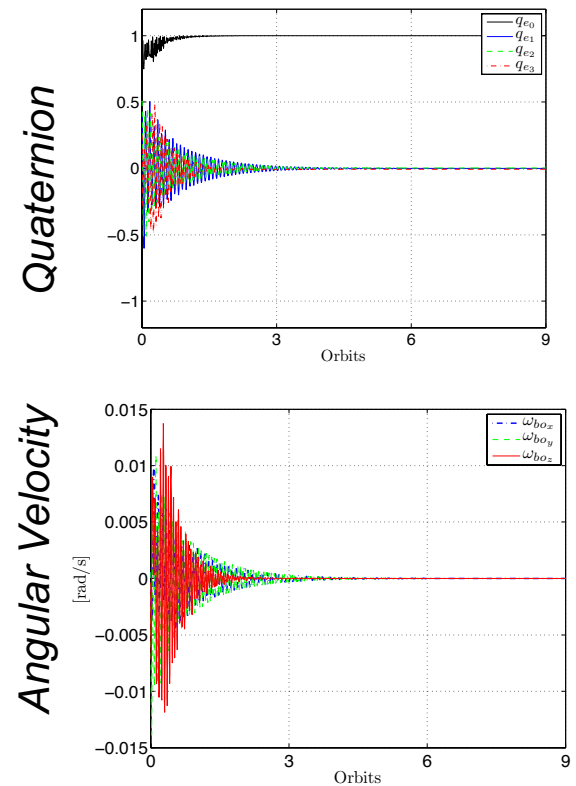
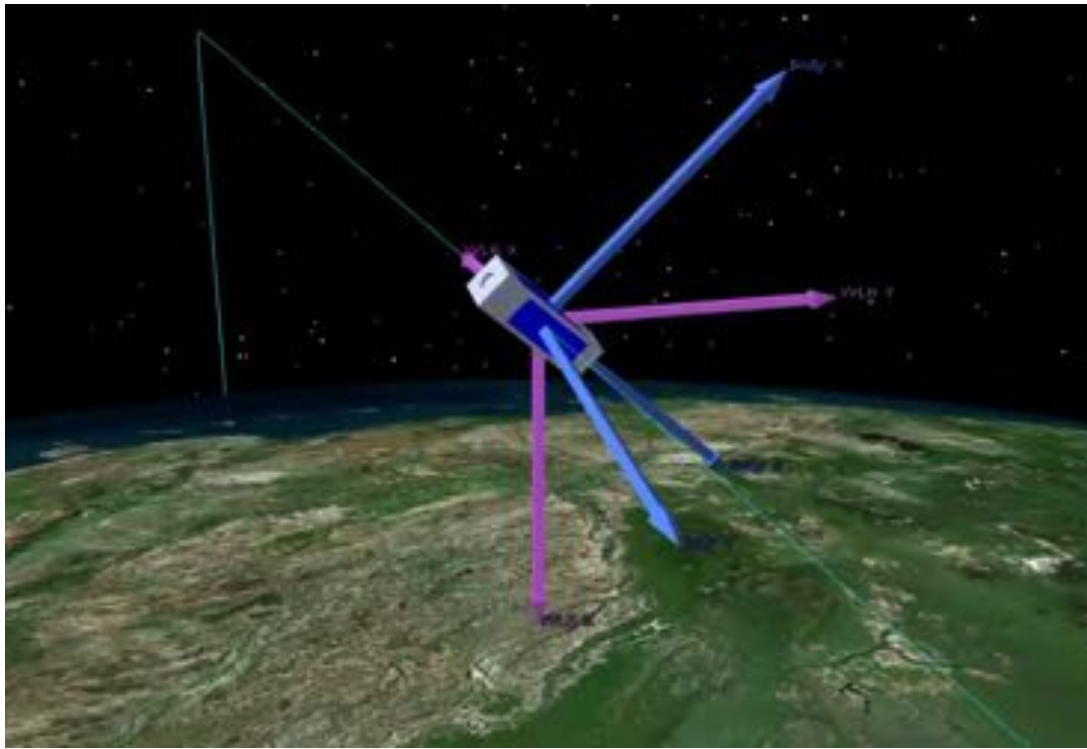
Using Aero-Drag for Attitude Maneuver in LEO

- Onboard shifting masses



$$\underline{\tau}_t = \underline{\tau}_M + \underline{\tau}_B$$

- Stabilization with shifting masses + magnetotorquers



[Ref: Chesi, Gong, Romano, Aerodynamic Three-Axis Attitude Stabilization of a Spacecraft by Center-of-Mass Shifting. *Journal of Guidance, Dynamics and Control.* 2016]

Seeking Exact Solutions of Rigid Body Motion

RESEARCH RATIONALE

- 1) Exact analytic solutions have a high theoretical value: very few exact solutions exist for the motion of a rigid body.
- 2) Even though numerical propagation compensate for this lack, exact solutions have also an important practical interest. In particular, they can be used
 - to solve problems where numerical propagation may fail (e.g. long term study of planetary rotation mechanics);
 - as comparison cases for the validation and error analysis of approximate algorithms;
 - as a basis to create new approximate algorithms.
- 3) Research motivated by Bilimoria/Wie paper

[Ref: KARL D. BILIMORIA and BONG WIE. "Time-optimal three-axis reorientation of a rigid spacecraft", *Journal of Guidance, Control, and Dynamics*, 1993.]

Partial Survey of Exact Solutions.

Euler, L.: Du mouvement de rotation des corps solides autour d'un axe variable, Mémoires de l'académie des sciences de Berlin. 14 (1758), 154–193.

Poinsot, L.: Théorie nouvelle de la rotation des corps. Journal Général des Sociétés et Travaux Scientifiques, Paris. 2 (1834)

Jacobi, C.G.J.: Sur la rotation dun corps. Comptes Rendus de l'académie des Sciences. 24, 97–106 (1849)

Morton, H.S., Junkins, J.L., Blanton, J.N.: Analytical Solutions for Euler Parameters. Celestial Mechanics and Dynamical Astronomy. 10(3), 287–301 (1974)

Deprit, A., Elipe, A.: Complete Reduction of the Euler-Poinsot Problem. The Journal of the Astronautical Sciences. 41(4), 603–628 (1993)

Lagrange, J.L.: Méchanique Analitique. Veuve Desaint, Paris (1788)

Kovalevskaya, S.V: Mémoire sur un cas particulier du problème de la rotation Académie des Sciences de l'Institut National de France, Paris. 31, 1–62 (1890)

Introduction. Rotational mechanics of a rigid body

Dynamic problem (Euler's equations)

$$I_1 \dot{p} = (I_2 - I_3) q r + m_1$$

$$I_2 \dot{q} = (I_3 - I_1) r p + m_2$$

$$I_3 \dot{r} = (I_1 - I_2) p q + m_3$$

Kinematic problem (Darboux equation)

$$\dot{R}_{NB} = R_{NB} \Omega(^B\omega_{BN})$$

$$\Omega(^B\omega_{BN}) = \begin{bmatrix} 0 & -r & q \\ r & 0 & -p \\ -q & p & 0 \end{bmatrix}$$

[The solution $R_{NB}(t) = R_{NB}(0) \exp\left(\int_0^t \Omega(\xi) d\xi\right)$ is only valid when the matrix $\Omega(t)$ commutes with its time integral]

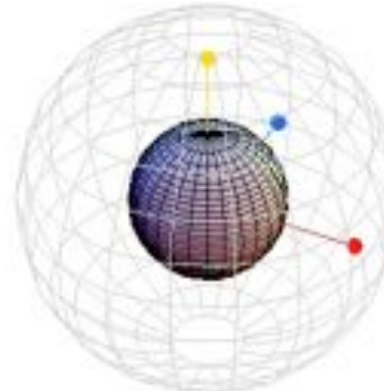
Spherically symmetric body subjected to constant torque

If torque is about the initial axis of rotation, the solution is trivial for both angular velocity and orientation:

1 dof uniformly accelerated system

But if torque is NOT about the initial axis of rotation, the orientation solution is much more complicated

```
time [s] = 0.  
T/I [s^-2] = [0, 0, 0]  
ω [s^-1] = [0, 2., 0]
```



X = red axis, Y = blue axis, Z=yellow axis

Spherically symmetric body subjected to constant torque

$$I_1 = I_2 = I_3 = I$$

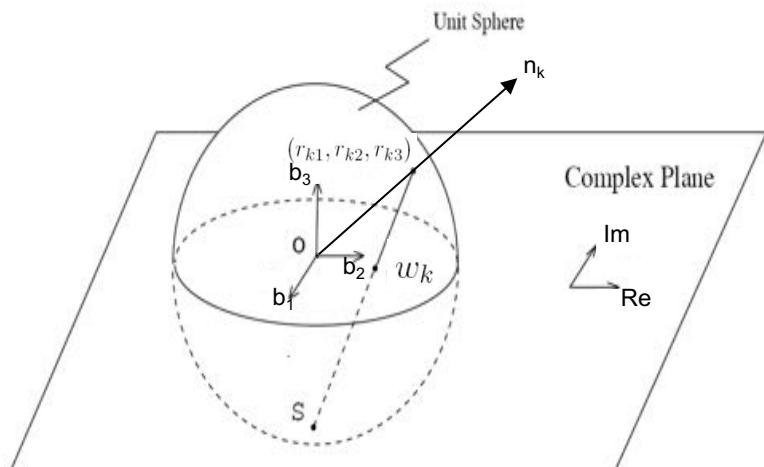
The dynamic problem is immediately solved

$$\dot{p} = 0 \quad p(t) = p_0$$

$$\dot{q} = 0 \quad \xrightarrow{\text{blue arrow}} \quad q(t) = q_0$$

$$\dot{r} = U \quad r(t) = r_0 + Ut$$

The kinematics is governed by the following differential equation for each of the three stereographic rotation variables



$$\dot{w}(t) = \frac{1}{2} (p_0 - iq_0) w(t)^2 - i(r_0 + Ut) w(t) + \frac{1}{2} (p_0 + iq_0)$$

Riccati-type Eq. with closed form solution



Spherically symmetric body subjected to constant torque

The solution of the kinematic problem is
(for each of the 3 stereo rotation variables)

$$w(t, c) = \frac{(1+i)\sqrt{U}}{3(p_0 - iq_0)} [6z + G(z, c)]$$

with

$$G(z, c) := \frac{2 {}_1F_1\left(\frac{3-\nu}{2}, \frac{5}{2}; z^2\right)(\nu-1)z^2 + 6 {}_1F_1\left(1-\frac{\nu}{2}, \frac{3}{2}; z^2\right)c\nu z - 3 {}_1F_1\left(\frac{1-\nu}{2}, \frac{3}{2}; z^2\right)}{{}_1F_1\left(-\frac{\nu}{2}, \frac{1}{2}; z^2\right)c + {}_1F_1\left(\frac{1-\nu}{2}, \frac{3}{2}; z^2\right)z}$$
$$z := \frac{(1+i)(r_0 + Ut)}{2\sqrt{U}}, \quad \nu := -1 - \frac{i(p_0^2 + q_0^2)}{4U}$$

Where ${}_1F_1(\alpha, \beta; \gamma)$ is the confluent hypergeometric function.

Efficient algorithms exist to numerically evaluate this function with arbitrary accuracy → no numerical propagation is needed.

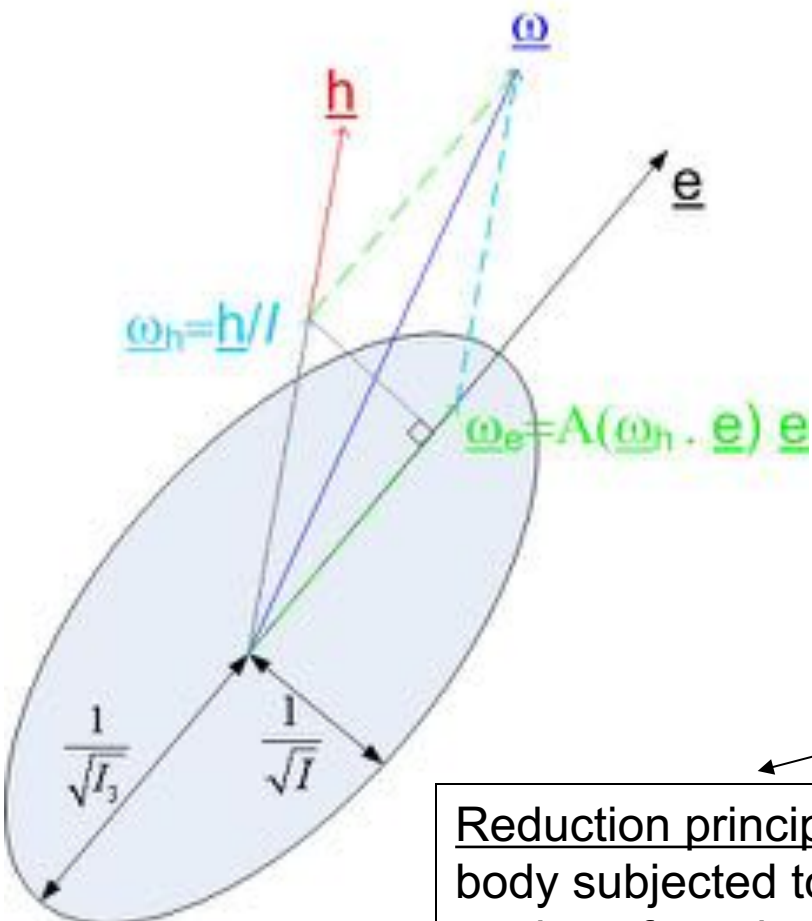
The solution can be easily expressed in terms of rotation matrix $\overline{R}_{SN}(t)$

[Ref: Romano, *Exact Analytic Solution for the Rotation of a Rigid Body having Spherical Ellipsoid of Inertia and Subjected to a Constant Torque, Celestial Mechanics and Dynamical Astronomy, 2008.*]

Axially symmetric body: reduction principle.

$$I_1 = I_2 = I \neq I_3$$

In order to extend the analytic results to an axially symmetric body, the reduction principle* is used



$$\underline{\omega} = \underline{\omega}_h + \underline{\omega}_e$$

$$\frac{h}{I}$$

$$A(\underline{\omega}_h \cdot \underline{e}) \underline{e}$$

$$h = I \underline{\omega}_h$$

$$A = \frac{(I - I_3)}{I_3}$$

the euler's equation can be written as

$$\dot{h} = I \dot{\underline{\omega}}_h = \underline{m}$$

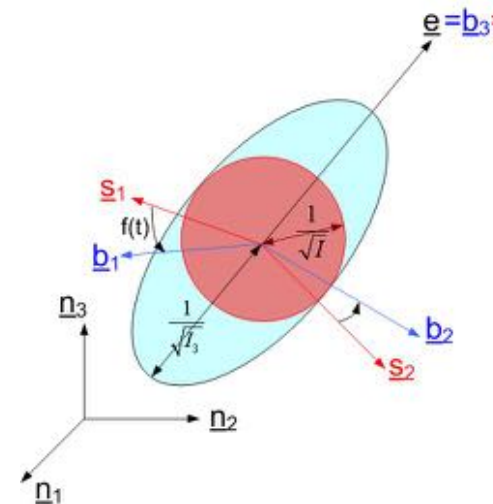
Reduction principle: the evolution of h of an axially symmetric body subjected to an external torque \underline{m} is analogous to the motion of a sphere with inertia I subjected to same torque.

* Hestenes, D., New Foundations for Classical Mechanics, Kluwer, 1999.

Axially symmetric body. Solutions.

Rotational motion of the axially symmetric body =

superposition of the motion of the virtual sphere relative to the inertial frame + rotation of the cylindrical rigid body (about its symmetry axis) relative to the virtual sphere



By using this approach, and the solution shown before for the spherical body, the analytic solutions is obtained for the motion of an axially symmetric body with:

- 1) Torque parallel to the symmetry axis and arbitrary initial angular velocity;
- 2) Torque and initial angular velocity perpendicular to the symmetry axis, with the torque being fixed with the body.

[Refs:

- 1) M. Romano, *Exact Analytic Solutions for the Rotation of an Axially Symmetric Rigid Body Subjected to a Constant Torque*, *Celestial Mechanics and Dynamical Astronomy*, 2008.
- 2) M. Romano, *Detumbling and Nutation Canceling Maneuvers with Complete Analytic Reduction for Axially Symmetric Spacecraft*, *Acta Astronautica*, 2010.
- 3) Ventura J., Romano M., *Exact Analytic Solution for the Spin-up Maneuver of an Axially Symmetric Spacecraft*. *Acta Astronautica*, 2014.]

]

Marcello Romano, mromano@nps.edu

Conclusions

I gave an overview of some of my research efforts from more applied to more theoretical ones, in particular on:

- 1) Spacecraft Engineering & Technology
-Development of HIL Test-beds for Spacecraft Proximity and Attitude Maneuvering (GN&C)
- 2) Orbital Robotics
-Design/test G&C Algorithms for S/C Proximity & Attitude Maneuvering
- 3) Space Flight Mechanics
-Using Residual Aero-Drag for Attitude Maneuvers
-Seeking & Using Exact Solutions of Rigid Body Motion

Thank you for your attention!